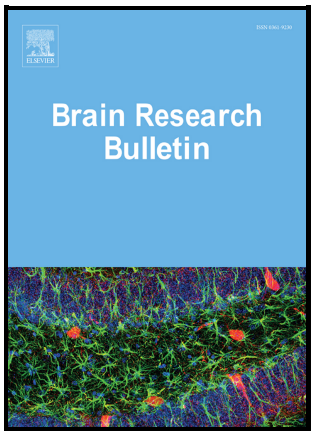

Hydromethylthionine rescues synaptic SNARE proteins in a mouse model of tauopathies: interference by cholinesterase inhibitors

Karima Schwab, Dilyara Lauer, Mandy Magbagbeolu, Franz Theuring, Anna Gasiorowska, Maciej Zadrozny, Charles R. Harrington, Claude M. Wischik, Grażyna Niewiadomska, Gernot Riedel

PII: S0361-9230(24)00088-1

DOI: https://doi.org/10.1016/j.brainresbull.2024.110955

Reference: BRB110955

To appear in: *Brain Research Bulletin*

Received date: 29 February 2024
Revised date: 14 April 2024
Accepted date: 17 April 2024

Please cite this article as: Karima Schwab, Dilyara Lauer, Mandy Magbagbeolu, Franz Theuring, Anna Gasiorowska, Maciej Zadrozny, Charles R. Harrington, Claude M. Wischik, Grażyna Niewiadomska and Gernot Riedel, Hydromethylthionine rescues synaptic SNARE proteins in a mouse model of tauopathies: interference by cholinesterase inhibitors, *Brain Research Bulletin,* (2024) doi:https://doi.org/10.1016/j.brainresbull.2024.110955

Hydromethylthionine rescues synaptic SNARE proteins in a mouse model of tauopathies: interference by cholinesterase inhibitors

Karima Schwab[1,2], Dilyara Lauer[2], Mandy Magbagbeolu[2], Franz Theuring[2], Anna Gasiorowska[3], Maciej Zadrozny[3], Charles R. Harrington[1,4], Claude M. Wischik[1,4], Grażyna Niewiadomska[3], Gernot Riedel[1*]

[1] School of Medicine, Medical Sciences and Nutrition, University of Aberdeen, Foresterhill, Aberdeen, AB25 2ZD, UK

[2] Institute of Pharmacology, Charité - Universitätsmedizin Berlin, Hessische Str. 3-4, 10115 Berlin, Germany

[3] Clinical and Research Department of Applied Physiology, Mossakowski Medical Research Institute, Polish Academy of Sciences, 02-106 Warsaw, Poland

[4] TauRx Therapeutics Ltd., 395 King Street, Aberdeen, AB24 5RP, UK

*Corresponding author: Gernot Riedel

Email: g.riedel@abdn.ac.uk

Phone: +44 1224437377

Key words: tau protein, Alzheimer's disease, HMTM, cholinesterase inhibitors, rivastigmine

Abstract

In clinical trials for Alzheimer's disease (AD), hydromethylthionine mesylate (HMTM) showed reduced efficacy when administered as an add-on to symptomatic treatments, while it produced a significant improvement of cognitive function when taken as monotherapy. Interference of cholinesterase inhibition with HMTM was observed also in a tau transgenic mouse model, where rivastigmine reduced the pharmacological activity of HMTM at multiple brain levels including hippocampal acetylcholine release, synaptosomal glutamate release and mitochondrial activity. Here, we examined the effect of HMTM, given alone or in combination with the acetylcholinesterase inhibitor, rivastigmine, at the level of expression of selected pre-synaptic proteins (syntaxin-1; SNAP-25, VAMP-2, synaptophysin-1, synapsin-1, α-synuclein) in brain tissue harvested from tau-transgenic Line 1 (L1) and wild-type mice using immunohistochemistry. L1 mice overexpress the tau-core unit that induces tau aggregation and results in an AD-like phenotype. Synaptic proteins were lower in hippocampus and cortex but greater in basal forebrain regions in L1 compared to wild-type mice. HMTM partially normalised the expression pattern of several of these proteins in basal forebrain. This effect was diminished when HMTM was administered in combination with rivastigmine, where mean protein expression seemed supressed. This was further confirmed by group-based correlation network analyses where important levels of co-expression correlations in basal forebrain regions were lost in L1 mice and partially re-established when HMTM was given alone but not in combination with rivastigmine. These data indicate a reduction in pharmacological activity of HMTM when given as an add-on therapy, a result that is consistent with the responses observed in the clinic. Attenuation of the therapeutic effects of HMTM by cholinergic treatments may have important implications for other potential AD therapies.

Introduction

Alzheimer´s disease (AD) is a growing health concern with yet no disease-modifying therapy; the only available treatments are symptomatic and include acetylcholinesterase inhibitors (AChEI), N-methyl-D-aspartate (NMDA) receptor antagonists *(1)* and recently approved anti-amyloid antibody therapies with aducanumab *(2–5)* and lecanemab *(6)*. AChEIs and NMDA receptor antagonists modulate brain function broadly in a non-specific manner and their therapeutic benefits tend to be short-lasting *(7)*. One disease-modifying treatment for AD is based on targeting tau aggregation with methylthioninium chloride (MTC) and its stably reduced form hydromethylthionine bis(hydromethanesulfonate) (HMTM; N3,N7,N7,N7-tetramethyl-10H-phenothiazine-3,7-diaminium bis (methanesulfonate)). The methylthioninium (MT) moiety exists in an equilibrium between oxidised (MT^+) and reduced (HMT) forms and HMT rather than MT^+ is the active species of HMTM that blocks tau aggregation and propagation *in vitro (8, 9)*. MT/HMT is able to reverse behavioural deficiencies and tau pathology in transgenic tau mice *(10–12)* and to halt cognitive decline and brain atrophy in mild/moderate AD patients in a Phase 2 clinical trial *(13, 14)*. MTC was found to facilitate tau clearance *in vitro* and in animal models of AD by acting on the ubiquitin-proteasome-system and on autophagy *(10, 15)*.

In addition to its activity as a tau aggregation inhibitor, MTC can exert several other beneficial effects on pathways relevant to neurodegenerative disorders *(16)*. It induces mitochondrial biogenesis; increases mitochondrial complex I-IV activity, thereby enhancing electron transport and provision of energy, and it activates NRF2-mediated antioxidant responses and inhibits microglial activation *(17–24)*. Using a proteomics approach, we have recently confirmed that HMTM influences oxidative phosphorylation and NRF2 and highlighted its influence on neurotransmission and metabolism *(25)*. Given this preclinical evidence, it was surprising that HMTM failed to show efficacy in a phase 3 trial in patients with mild to moderate AD *(26)*. However, secondary analyses revealed a potential interference of symptomatic treatments with HMTM *(26, 27)* and the inhibitory effects of AChEIs on HMTM-related improvement of cognitive function and brain volume could not be overcome simply by increasing the concentration of HMTM *(28)*. The efficacy reported for MTC in a phase 2 trial in which subjects receiving AChEI or NMDA receptor antagonists were either excluded or had undergone a wash-out period before receiving MTC *(14)* would be consistent with a negative interaction.

It is conceivable that in response to long-term treatment with symptomatic drugs such as AChEIs, a homeostatic adaptation within neuronal networks is likely to occur. Such adjustments of neuronal systems have been associated with neurodegenerative disorders, where changes in neuronal interactions between different brain areas and functionally connected brain networks have been described *(29–34)*. On the other hand, immunocytochemistry of post-mortem tissue confirms that synapse loss, possibly caused by tau aggregation, is the strongest correlate for cognitive decline in AD, and often precedes clinical manifestations (for review, see *(35, 36)*). We therefore explored whether alterations in pre-synaptic components underlying disease progression can be corrected by HMTM and predicted that pre-exposure to AChEIs would interfere with this efficacy. Consequently, we measured the abundance of several synaptic, SNARE (soluble N-ethylmaleimide-sensitive factor attachment protein receptor) and non-SNARE proteins, as these are crucial mediators of synaptic function *(37)*.

We have reported in a tau-transgenic model of AD, Line 1 (L1), that chronic reduction of AChE considerably altered a broad range of brain responses to HMTM *(24)*. Multiple loci/systems for such putative interactions, including hippocampal acetylcholine levels, glutamate release, mitochondrial activity and levels of synaptic proteins were presented and the beneficial impact of HMTM treatment appeared to be blunted by pre-treatment with the AChEI rivastigmine *(24)* . In this study, we set out to determine the pre-synaptic changes in protein levels as surrogate indicators for structural synaptic alterations and for functional linkage of selected brain areas which may underlie these negative interactions. Both the SNARE proteins syntaxin-1, SNAP-25 and VAMP-2, as well as the non-SNARE

proteins synaptophysin-1, synapsin-1 and alpha-synuclein were selected due to their particular importance for synaptic vesicle assembly/mobilisation/fusion *(38–42)*. L1 mice and wild-type controls were pre-treated with rivastigmine, with HMTM treatment started later as an add-on therapy. This study design was chosen to mimic the clinic where patients are chronically treated with symptomatic drugs, e.g., AChEI, before receiving HMTM. The treatment regimens for HMTM in the current pre-clinical study were based on successful lowering of tau pathology and on behavioural phenotype rescue in L1 mice *(12)*. The core groups received high doses of rivastigmine or HMTM and a combination of the two drugs, while satellite groups received low doses of both drugs and drug combinations attempting to provide a mechanistic understanding of effects detected in the core groups. For this exploratory study, the primary endpoints have been the levels of abundance for six selected synaptic proteins in six brain regions.

Materials and Methods

Animals

All animal experiments were carried out in accordance with the European Communities Council Directive (63/2010/EU) and approved by the Polish Law on the Protection of Animals and National Institute of Health's Guide for Care and Use of Laboratory Animals (Publication No. 85-23, revised 1985) and comply with the ARRIVE guidelines 2.0 *(43)*.

Female homozygous transgenic L1 and wild-type NMRI litters were generated as previously described *(44)*. L1 mice overexpress the repeat domain 296-390 of the longest human CNS tau isoform (htau40) fused with an N-terminal endoplasmic reticulum-directing signal sequence and inserted into the murine *Thy1* cassette for neuronal expression. The truncated repeat domain of tau overexpressed in L1 corresponds to the core fragment of tau in the paired helical filament (PHF) found in AD brain tissue. L1 mice show evidence of neuroanatomical spread and amplification of tau pathology with age that result in prominent cognitive impairments reminiscent of AD. A detailed characterisation of these transgenic mice was reported earlier, and male and female mice show similar behavioural and pathological phenotypes *(44, 45)*.

Mice were bred commercially (Charles River, UK) in positive-pressure isolators in specific pathogen-free conditions. They were delivered to the experimental holding areas of the investigating institution (Nencki Institute, Warsaw, Poland) one month before testing for acclimatisation. They were housed, by genotype, in small colonies up to five mice in open housing (Type III, 382 x 220 mm) with corn cob bedding and paper strips and cardboard tubes as enrichment (cleaning rota once per week). Holding rooms were on constant temperature (20-22°C), humidity (60-65%), and air exchange rate (17-20 changes/h) with 12 hours light/dark cycle (lights on at 6 am, simulated dawn). Animals had free access to food and water. A total of 118 mice were used (for group sizes, see Table 1) and were 5-7 months old when they entered the study based on previously established phenotypes of these mice *(44)*. Animal body weights were determined once prior to dosing for assignment to treatment based on equal group weight (week 0) and then five times per week during the dosing phase (weeks 1-11). The weekly body weight (average of 5 days) was used for body weight change calculations (percent change of week x relative to week 0). During the first two weeks of treatment, we performed visual observations for anomalous behaviour, but these were not quantified. Experimenters were not blinded during allocation, conduct of the experiment and behavioural assessment.

Drugs and treatments

N3,N7,N7',N7'-tetramethyl-10*H*-phenothiazine-3,7-diaminium bis (methanesulfonate) (leuco-methylthioninium bis(hydromethanesulfonate); HMTM; hydromethylthionine mesylate) was supplied by TauRx Therapeutics Ltd., Aberdeen UK. Rivastigmine was purchased from Tocris Bioscience (Bristol, UK, #4440). The interference by the AChEI rivastigmine on the efficacy of HMTM was modelled in an 11-week study which included two phases. During phase 1 (weeks 1-5), mice received rivastigmine at 0.5 mg/kg/day and, during phase 2 (weeks 6-11), mice received both rivastigmine (0.5 mg/kg/day) and HMTM (15 mg/kg/day). Control mice received vehicle throughout the study (weeks 1-11); HMTM mice received only HMTM during phase 2 (6-11); and another treatment group received only rivastigmine (weeks 1-11). Satellite groups of L1 mice were treated with lower doses of rivastigmine (0.1 mg/kg/day), HMTM (5 mg/kg/day), and their combination and were treated simultaneously to the core groups. Treatment details and individual group sizes are given in Table 1.

Table 1: Treatment groups and cohort sizes for wild-type NMRI and L1 tau-transgenic mice. All drug doses are expressed in mg/kg/day. Three mice (labelled with *) were excluded from experiment reducing N in these groups. Riva: rivastigmine; COMB = combination of rivastigmine and HMTM.

Group	Name-dose	Treatment phase 1 (Weeks 1-5)	Treatment phase 2 (Weeks 6-11)	Genotype	Number of mice
Core	Vehicle	Vehicle	Vehicle	NMRI	9
				L1	9
	HMTM-15	Vehicle	HMTM-15	NMRI	10
				L1	9* (8)
	Riva-0.5	Riva-0.5	Riva-0.5	NMRI	9* (8)
				L1	9* (8)
	COMB-0.5/15	Riva-0.5	Riva-0.5 + HMTM-15	NMRI	10
				L1	9
Satellite	HMTM-5	Vehicle	HMTM-5	L1	9
	Riva-0.1	Riva-0.1	Riva-0.1	L1	9
	COMB-0.1/5	Riva-0.1	Riva-0.1 + HMTM-5	L1	9
	COMB-0.1/15	Riva-0.1	Riva-0.1 + HMTM-15	L1	9
	COMB-0.5/5	Riva-0.5	Riva-0.5 + HMTM-5	L1	8

Drugs were administered via oral gavage at a volume of 5 ml/kg of body weight daily for 5 days per week (Monday to Friday) in the morning between 8 and 10 a.m. Nitrogen-sparged deionised water was used as vehicle for both drugs. HMTM was administered within 20 min of dissolution while rivastigmine aliquots were used for 2 – 3 weeks and stored at 4ºC. Treatment regimen and dose selection for HMTM were based on successful lowering of tau pathology and on behavioural phenotype rescue in the tau-transgenic mice *(12)*. The dose of rivastigmine (0.5 mg/kg/day) was chosen based on successful inhibition of cholinesterase in cortex and hippocampus – the most affected regions in AD brains – and on rescue of cognitive deficits in mice and rats *(46–49)*. This dose is comparable with oral dosages administered to AD patients (1.5 mg capsules twice a day (see *(50)* for dose conversion between human and mouse).

Animal sacrifice and brain tissue collection

Terminally anaesthetised mice (sodium pentobarbital, 150 mg/kg) were transcardially perfused with 30 ml PBS (0.1 M, pH 7.4) containing heparin (0.1 ml of heparin solution (WZF 5000 IU/ml, Polfa

Warszawa SA, Warsaw, Poland) for 100 ml PBS), followed by perfusion with 50 ml of 4% paraformaldehyde with 15% saturated picric acid in 0.1 M PBS pH 7.4 and another 30 ml of 5% glycerol with 2% DMSO in 0.1M PBS (pH 7.4). Skulls were then immediately dissected and whole brains retrieved. The left hemisphere of all subjects was dissected, incubated in formalin, embedded in paraffin (see below), and used to quantify the abundance of synaptic proteins by immunohistochemistry. The right brain hemisphere was frozen and used to perform immunohistochemical tau localisation studies. Tissue collection was performed over three days post treatment.

Tissue sectioning, immunohistochemistry, microscopy, and tissue analyses for the quantification of synaptic proteins

Left brain hemispheres from formalin were transferred to tap water for 30min and thereafter dehydrated in a tissue processor (Epredia™ Citadel 2000, Thermo Fisher Scientific, Waltham, MA, USA) in a series of ethanol solutions with increasing concentrations (1h 70% (v/w) ethanol, 1h 96% (v/w) ethanol, 3x 1h 100% (v/w) ethanol), followed by 2x incubation in Neoclear (#109843, Merck, Darmstadt, Germany) for 30min, and 2h in paraffin type 6 (12066669, Thermo Fisher Scientific) and at least 5h in paraffin type 9 (12076669, Thermo Fisher Scientific). At the end, tissue was embedded in paraffin (type 9) using a tissue embedder (Leica® EG1150 Modular Tissue Embedding Centre, Leica Biosystems, Nussloch, Germany).

Paraffin-embedded brain tissue was sectioned at 5-µm thickness at the desired brain levels (Bregma 0.86 ± 0.24 mm for front brain and -2.7 ± 0.24 mm for midbrain) in accordance with the Mouse Brain Stereotaxic Atlas *(51)* using a rotary microtome (Microm HM325, Leica Biosystems). Regions of interest were pre-defined as hippocampal CA1 (CA1), visual cortex (VC), primary motor cortex (MC), medial septum (MS), vertical limb of the diagonal band of Broca (VDB) and nucleus accumbens (AcB). The levels of syntaxin-1 (SNTX-1), synaptosomal-associated protein 25 (SNAP-25), vesicle-associated membrane protein 2 (VAMP-2), synaptophysin-1 (SYNPY-1), synapsin-1 (SYN-1) and alpha-synuclein (A-SYN) were quantified in these six regions.

Brain sections from left hemispheres were collected on SuperFrost™ glass slides (Thermo Fisher Scientific). Four sections from front brain were collected on one glass slide and four sections from midbrain were collected on a second glass slide, resulting in two slides for each mouse and antibody. Each section series was 50-60 µm apart from each other to avoid reanalyses of the same cells/synapses.

Slide series (for each antibody and region) were randomised over seven immunohistochemistry staining boxes in a way that each box contained at least one slide from each of the thirteen study groups, and the same randomisation scheme was used throughout. For immunohistochemistry, the protocol described earlier was applied *(52)*. Briefly, sections were dewaxed, rehydrated, boiled in citrate buffer (10 mM, pH 6.0), washed with distilled water, and incubated in 0.3% (v/v) hydrogen peroxidase solution for 5 min. After washing three times in PBS (pH 7.4) and 20 min blocking in 0.1 % (w/v) bovine serum album (BSA)-PBS, sections were incubated for 1 h in primary antibody, washed three times in PBS, incubated for 30min in biotinylated secondary antibody (polyclonal goat anti-rabbit, BA-1000, or polyclonal goat anti-mouse, BA-9200, both from VECTOR labs, Burlingame, CA, USA; diluted 1:200) and washed a further three times in PBS. Thereafter, sections were incubated for 30 min in VECTASTAIN® ABC-HRP (PK-4000, VECTOR labs), washed shortly three times in PBS, incubated with ImmPACT DAB (3,3′-diaminobenzidine tetrahydrochloride) peroxidase (HRP) substrate (SK-4105, VECTOR labs), washed shortly in distilled water, dehydrated, and mounted with coverslips. Primary and secondary antibodies were diluted in PBS containing 0.1 % (w/v) BSA. Details for primary antibodies used are given in Table 2.

Table 2: List of antibodies. SNAP-25: synaptosomal-associated protein 25, VAMP-2: vesicle-associated membrane protein 2, mAb: monoclonal antibody, pAb: polyclonal antibody.

Antibody	Antigen/epitope	Source	ID	Dilution
Syntaxin-1 (mAb)	Crude synaptic preparation from human brain	Abcam	ab112198	1:2,000
SNAP-25 (mAb)	Crude synaptic preparation from human brain	Biolegend	805001	1:5,000
VAMP-2 (pAb)	Residues 2-17 of rat VAMP-2	Synaptic Systems	104202	1:1,000
Synaptophysin-1 (pAb)	Residues 301-313 of human synaptophysin-1	Synaptic Systems	101002	1:250
Synapsin-1 (mAb)	Proline rich D-domain of rat synapsin-1	Synaptic Systems	106001	1:20,000
Alpha-synuclein (mAb)	Synthetic peptide surrounding Glu105 of mouse alpha-synuclein	Cell Signaling	4179	1:2,000
s1D12 (mAb)	Human tau; epitope - residues 337-355	Genting TauRx Diagnostic Centre	s1D12	1:100

Sections were viewed by light microscopy using an Axio Imager M1 microscope (Carl Zeiss, Jena, Germany). The investigator was blinded to all treatment details aside from the antibody. Pictures were taken from the pre-defined regions (MS, VDB, AcB and MC from front brain, VC and CA1 from midbrain) at 200x- magnification and saved as jpg. The relative abundance of the synaptic proteins was measured as integrated density in 8-bit images by a different investigator, also blinded to all treatment details (aside from the antibody), using the ImageJ tool (version 1.48v, NIH National Institutes of Health, Bethesda, MD, USA) at default threshold settings. Integrated density values were exported into an Excel data sheet. For each individual mouse, the mean over the four analysed sections for each region and antibody was calculated and used for analyses. Raw data for protein abundance are displayed in the supporting information (Supplementary Table 1).

Tissue sectioning, immunohistochemistry, and microscopy for localisation of tau

Frozen brain tissue from the right hemispheres was defrosted from -80 to -20°C and then further to 4°C in steps of 6 hours each and immersed into 4% PFA in 0.1 M PBS for 5 days and stored at 4°C. Then, brains were moved to 70% ethanol for 2 days and processed in a series of ethanol solutions of increasing concentration until pure water-free alcohol. Next, the hemispheres were exposed to xylene three times and finally infiltrated with histological paraffin wax twice. Paraffin blocks of tissue were stored at room temperature.

The paraffin-embedded brain tissue was sectioned coronally at 6 µm at preselected regions (Bregma 1.94 mm to -2.7 mm) in accordance with the Mouse Brain Stereotaxic Atlas *(51)* using a rotary microtome (Microm HM325, Leica Biosystems, Nussloch, Germany). Sections from each mouse were collected on SuperFrost™ glass slides (Thermo Fisher Scientific, Waltham, MA, USA). Immunohistochemical staining started with dewaxing steps (xylene 1, xylene 2, xylene 3, 1: 1 xylene:

ethanol, 100% ethanol, 100% ethanol, 96% ethanol, 96% ethanol, 70% ethanol, 50% ethanol) and rehydration in tap water twice, each for 1 min. Exposure of the antigen was performed in a citric acid solution (10 mM, pH 6.0) heated to 95-98°C for 30-35 min and cooled slowly to room temperature. Subsequently, the tissue was washed twice with distilled water and then treated with 3% hydrogen peroxide in methanol for 15 min at room temperature. Sections were washed with water for 10 min and with 0.1 M PBS (pH 7.4) for 5 min and incubated at 4°C overnight in anti-tau s1D12 antibody solution (diluted in 3% BSA in 0.1 M PBS). On the next day, after washing three times for 5 minutes in 0.1 PBS with 0.3% Triton X 100 (PBST), the tissue was incubated with a secondary goat anti-mouse antibody conjugated with horseradish peroxidase (HRP) at a concentration of 1:100 (AP124, Merck) in a buffered (0.1 M PBST) solution of 5% normal goat serum (S-1000-20, VECTOR labs) and 1% BSA for 1 hour at room temperature. The sections were then washed three times for 5 min in 0.1 M PBS. DAB (Sigma-Aldrich, St. Louis, MO, USA) with H_2O_2 and NiSO4 at concentrations of 0.025%, 0.0125% and 0.04%, respectively was used to visualize the primary-secondary antibody complex. After drying, the samples were mounted using DePeX (Serva, Heidelberg, Germany). Two control stains were performed omitting the first or second antibody and no immuno-positive reaction was observed for any of these control slides. Sections stained against tau were analysed using a bright field microscope (Nikon Eclipse Ni-E 400, Tokyo, Japan) equipped with the Nikon DS-Ri2 camera and NIS image analysis software. Microscopic images taken from the pre-defined brain regions at 100x magnification were digitalized and saved as TIFF files.

Data analyses

Data for body weight is expressed as group mean with standard deviation (± S.D.) and statistical analyses were conducted using 2-way ANOVA with time and genotype x treatment or time and treatment as independent variables.

Values for synaptic protein abundance were transformed to z-scores in Microsoft Excel (version 16.0 Office 365, Microsoft, USA) using the formula

$$z = \frac{\mathrm{x} - \mu}{\sigma}$$

where z is the z-score, x is the observed value, μ and σ are the group mean and the standard deviation of the reference group for that given protein. Vehicle-treated, wild-type mice were used as the reference group. Values were then plotted individually with group mean and S.D. Cohort sizes are indicated in Table 1 and in the figure legends. GraphPad Prism software (version 8.00; GraphPad Software Inc., San Diego, CA, USA) was used for statistical analyses and for generation of graphs, as well as for generation of expression / correlation heatmaps and estimation plots. Differences between groups were analysed using 1-way or 2-way ANOVA, followed by post-hoc comparison with Bonferroni corrected Student's t test. The differences were considered statistically significant for $p \leq 0.05$ and only significant outcomes are reported in the text.

For generation of expression heatmaps, z-scored data (from above) was transcribed to GraphPad and assigned a colour depending on their relative location to the population average: values near the population average are shown in black, values below the average are displayed in red, while values above the average are presented in green. The colour intensity indicates the distance from the population average (dark colours are closer to the average than light colours). Correlation heatmaps were calculated based on z-scored data in GraphPad and Pearson´s correlation was applied to the data set with resulting R- and *p*-values plotted in Figures. Positive correlations were coloured blue, inverse correlations were labelled yellow and when no correlation was seen (R close to 0) then the correlation value was displayed in white. Corresponding *p*-values were coloured purple if significant ($p < 0.05$) and lack of significancy

is shown in white. Estimation plots – for determination of drug effect sizes – were also created using GraphPad.

Results

In clinical trials for AD, HMTM showed reduced efficacy when administered as an add-on to symptomatic treatments with either AChEIs and/or memantine, while it produced a significant improvement of cognitive function when given as monotherapy. The current study design in mice was chosen to mimic this clinical study design for rivastigmine with HMTM; HMTM treatment regimens were based on successful lowering of tau pathology and on behavioural phenotype rescue in L1 mice *(12)*. and has, as primary readout, the histopathological quantification of six selected synaptic proteins in predefined brain areas. The study was conducted for 11 weeks, with mice treated with rivastigmine and HMTM added later.

Mouse body weight differs between genotype and treatment cohorts

There was a global difference between body weights for wild-type and L1 mice considering all 13 study groups at the beginning of the study (37.7g ± 3.0g for wild-type and 30.9g ± 3.0g for L1 (mean with SD), $p < 0.0001$). Two mice were euthanised because of poor tolerance of the oral gavaging procedure (one L1 mouse treated with HMTM-15 on day 38 and one NMRI wild-type mouse treated with Riva-0.5 on day 53) and a third mouse was euthanised due to body weight loss that exceeded 15% following animal welfare recommendations (L1 mouse treated with Riva-0.5 on day 46). These mice were excluded from further analyses (Table 1); the remaining mice showed no signs of unexpected adverse events or distress. Each of the treatments led to initial body weight reductions for the 8 core groups (Fig. 1A, effect of time F (5.5, 346); $p < 0.0001$), which plateaued after 4-5 weeks of treatment and the reduction was generally more pronounced in L1 compared to wild-type mice (effect of genotype x treatment F (7, 63) = 3.18; $p = 0.006$). Additionally, there was a significant interaction effect between time, genotype, and treatment (F (77, 693) = 1.655; $p = 0.0007$) confirming the weight loss differed over time in both genotypes and was dependent on drug exposure. By the end of the study, no differences between treatments were seen any longer (Fig. 1B), but genotype-related differences persisted, and L1 mice still showed greater body weight reductions compared to wild-type mice independent of the drug applied (effect of genotype: F (1, 63) = 7.761; $p = 0.007$). A similar time course was observed for the five L1 satellite groups (Fig. 1C and D).

These results support the tolerance of mice to HMTM and rivastigmine when each drug was given alone or in combination at daily doses up to 15 mg/kg/day for HMTM and 0.5 mg/kg/day for rivastigmine.

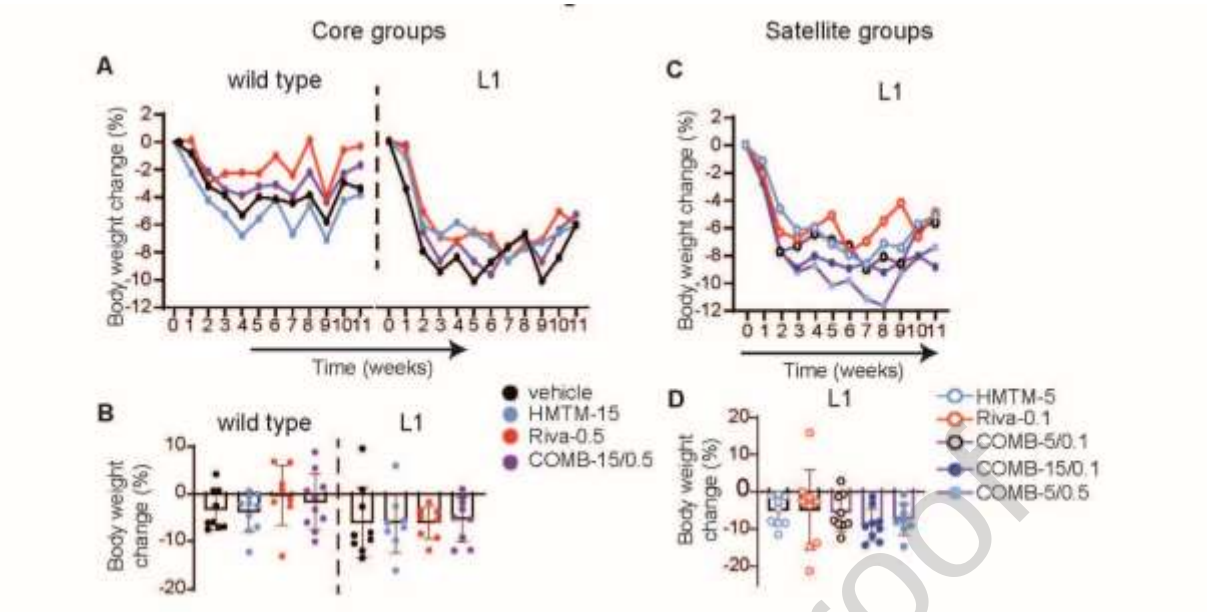

Fig. 1 Body weight changes for L1 and wild-type mice. Weekly average body weight change (A and C), expressed as the percentage change relative to the pre-dose body weight (each weekly point is calculated as an average of five measurements obtained during each given week), and total body weight change (B and D), expressed as the percentage change after 11 weeks of treatment relative the pre-treatment weight, for wild-type and L1 core groups (A-B) and L1 satellite groups (C-D). For clarity, values are shown as group mean only (A and C), and the total body weight change shown as mean and S.D (B and D). Statistical analyses were conducted using 2-way ANOVA with time and genotype x treatment (A/C) or time and treatment (B/D) as independent variables.

Synaptic protein expression in L1 mice differs from wild-type in a protein and brain region specific manner

We first established histologically that transgenic human tau accumulated in synapses in L1 mice. Immunopositive tau labelling presented as puncta clearly visible in CA1 and MC, but also in the basal forebrain regions MS and VDB, and to a lower extent in VC and AcB (Fig. 2A). This confirms tau accumulation in synapses of these regions in L1 mice. By contrast, wild-type mice were devoid of any such tau-staining. A detailed quantification of tau staining will be reported separately.

We quantified several synaptic proteins as an indicator for structural synapse alterations. The abundance of the SNARE proteins SNTX-1, SNAP-25, and VAMP-2, as well as the non-SNARE proteins SYNPY-1, SYN-1 and A-SYN was measured in regions of interest as integrated density in immunohistological micrographs (representative images are shown in Fig. 2B). Data were converted into z-scores, normalised to tissue from vehicle-treated wild-type mice (for each given protein in each of the regions individually), and displayed as scatter plots or expression heatmaps (Fig. 3-5 and 7).

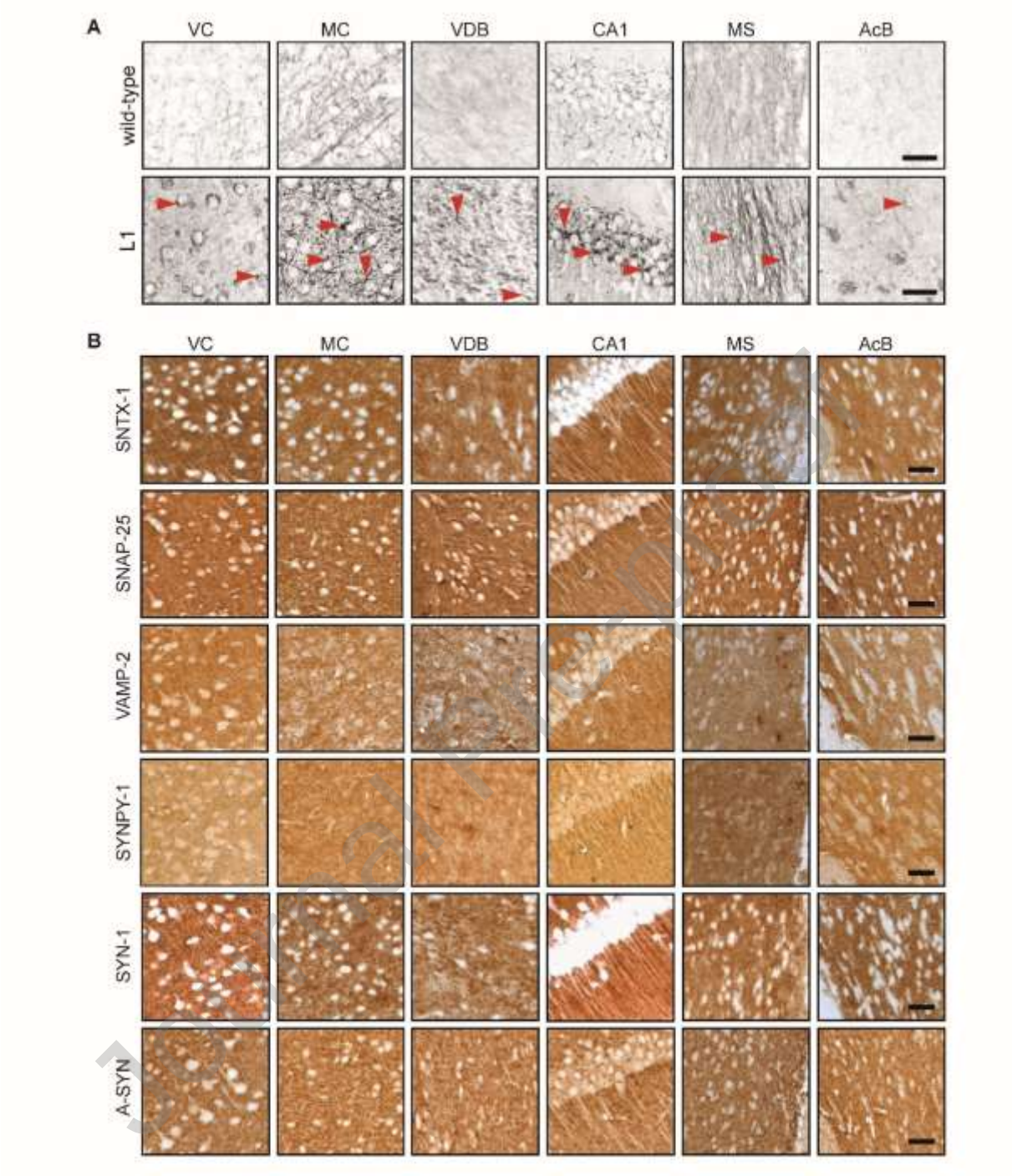

Fig. 2 Synaptic immunohistochemistry in vehicle-treated L1 and wild-type mice. Tau immunoreactivity with the antibody s1D12 showed prominent synaptic staining in L1 but not wild-type mice (A). Representative micrographs of a vehicle-treated wild-type mouse (ID 43, for protein abundance raw data see Supplementary Table 1 in the supporting information) showing high abundance of SNTX-1, SNAP-25, VAMP-2, SYNPY-1, SYN-1, and A-SYN in synapses (B). Analysed brain regions included the visual cortex (VC), the primary motor cortex (MC), the vertical limb of the diagonal band of Broca (VDB), hippocampal CA1 region (CA1), the medial septum (MS), and the nucleus accumbens (AcB). Scale bars: (A) 50 µm and (B) 100 µm.

In vehicle-treated cohorts, abundance of synaptic proteins was similar between genotypes for most proteins and examined brain areas (Fig. 3A). To visualise expression patterns, individual protein abundance z-scores are expressed as heatmaps, clustered by brain region, in wild-type (Fig. 3B) and L1 mice (Fig. 3C). Individual cells in each heatmap represent the z score for individual mice (9 wild-type and 9 L1 mice). In wild-type AcB for example, A-SYN values were below the average for three mice (mice #1, #3 and #8: red colour), near the average for three mice (mice #5, #6 and #9) and above the average for the other three mice (mice #2, #4 and #7). In contrast, with L1 mice AcB, A-SYN values were below the average for two mice (mice #1 and #2), near the average for three other mice (mice #3, #4 and #5) and above the average for the remaining four mice (mice #6, #7, #8 and #9: green colour). When group medians for each genotypes are plotted, the overall abundance of the six synaptic proteins of interest were lower in CA1 and VC (Fig. 3D, red cluster), but greater in MS, VDB and AcB (Fig. 3D, green cluster) for L1 compared to wild-type mice and, in general, protein expression in L1 was significantly different from wild-type mice (effect of genotype $F(1, 576) = 8.64$; $p = 0.0034$).

To explore whether protein abundance for the given proteins differed between regions and are dissimilar in wild-type and L1 mice, a different normalisation approach was taken. Unlike the analysis of the data above, where normalisation within the same protein and brain area was applied, the second normalisation approach used the VC values as reference for all other regions, as the VC (but also the CA1 region) showed the largest similarity between genotypes and treatments in our mice and is known to be the last region impacted by tau pathology in AD brains *(53)*. In wild-type mice, levels of SNTX-1 and VAMP-2 were reduced in MS and VDB but unchanged in CA1, MC and AcB (Supplementary Fig. 1). For SNAP-25 and SYNPY-1, levels were lower in VDB, greater in AcB, and not different in CA1, MC and MS. SYN-1 was lower in MS, VDB and AcB, but unchanged in CA1, and MC. A-SYN showed the same pattern of expression as SYN-1 except for AcB, where its expression was greater than, for example, in VC or MC. For L1 mice, all proteins showed the same region-specific behaviour seen in wild-type mice.

Taken together, these results provide compelling evidence of two features. (i) Differential levels of each protein in regions of interest in both genotypes. For example, the SNARE proteins SNTX-1 and VAMP-2 had low protein abundance in MS and VDB, but moderate abundance in the remaining brain regions, while for example A-SYN also showed low protein abundance in MS and VDB but heightened expression in AcB. (ii) A change in the level of proteins was found for L1 and this was region-specific, such that protein abundance was decreased in cortical and increased in subcortical structures (Fig. 3D).

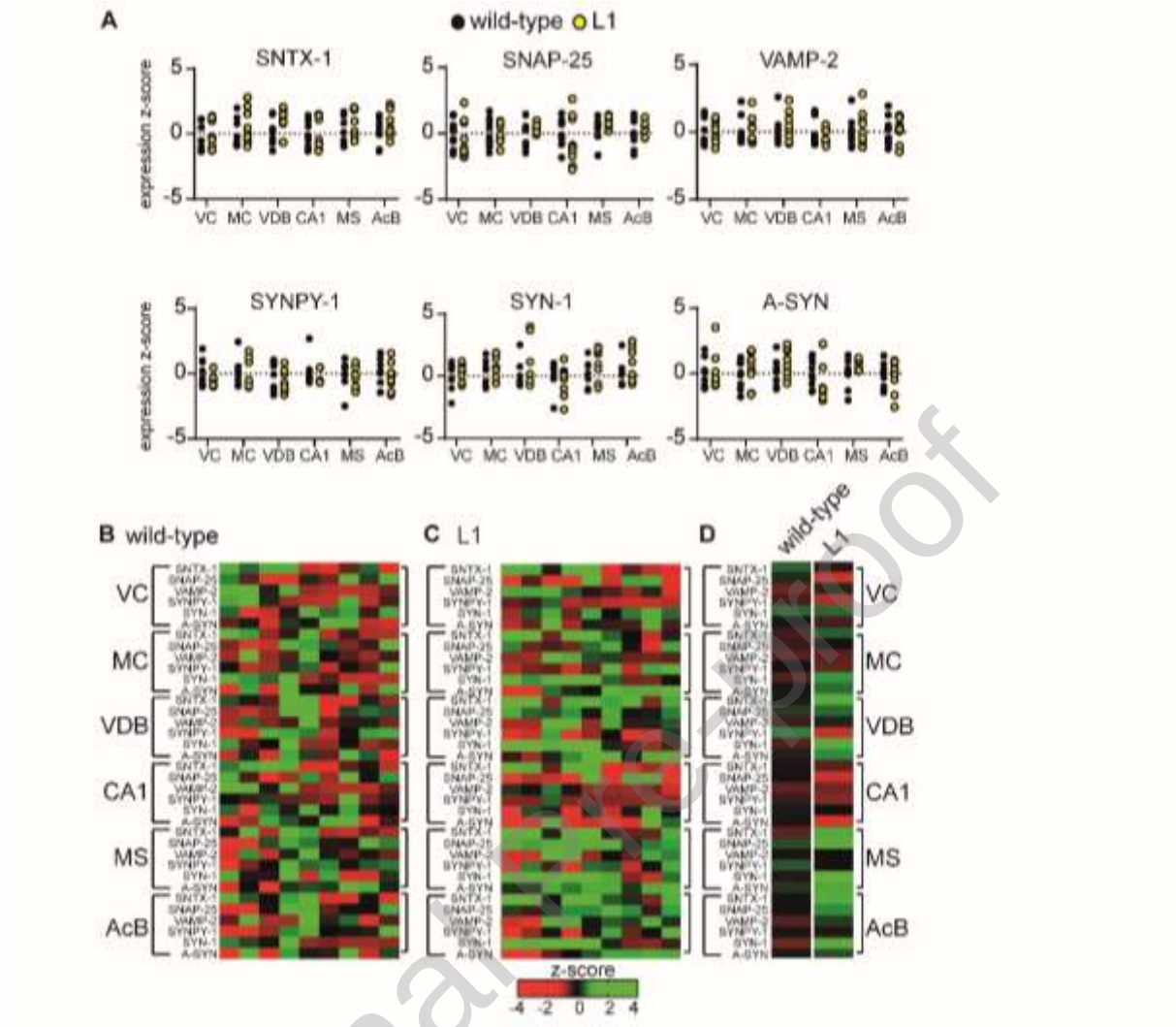

Fig. 3 Effect of the genotype on expression of synaptic proteins in vehicle-treated L1 and wild-type mice. Abundance (z-scores) of the synaptic proteins SNTX-1, SNAP-25, VAMP-2, SYNPY-1, SYN-1, and A-SYN in regions of interest, shown as scatter plots (A). To visualise expression patterns, individual protein abundances were converted into expression heatmaps organised by region of interest in wild-type (B) and L1 mice (C); each column depicts a different individual (9 mice per genotype). Group medians for each protein directly comparing wild-type and L1 mice treated with vehicle (D).

Region-specific effect of HMTM, Riva and their combination

For the core groups, the effect of therapeutic doses of AD treatments (vehicle, HMTM-15, Riva-0.5 and COMB-15/0.5) on this phenotype was examined next (Fig. 4). To visualise region-specific expression patterns, protein abundance z-scores were averaged to create a region-specific protein value for each of the given six region. These are shown as expression heatmaps for individual mice in wild-type (Fig. 4A) and L1 cohorts (Fig. 4B), as well as group medians (Fig. 4C).

In wild-type mice, protein expression is unaffected following treatment with HMTM-15 and Riva-0.5 except for MC (greater expression with Riva-0.5), CA1 (lower expression with Riva-0.5) and AcB (greater expression with HMTM-15 and COMB-15/0.5). In L1 mice compared to vehicle-treated wild-types, protein expression is greater in MC/VDB/MS following vehicle, HMTM-15 and Riva-0.5 treatment, but lower in these same three regions following treatment with COMB-15/0.5. By contrast, protein expression was lower compared to vehicle-treated wild-types in CA1 following vehicle, HMTM-15 and Riva-0.5 treatment, but corrected to vehicle-treated wild-type levels in the same region following treatment with COMB-15/0.5. These changes when averaged over all regions, however, did not reach statistical significance for either genotype (Fig. 4C). Note that the VC region showed the largest similarity between genotypes and treatments and was therefore used for the alternative normalisation approach as stated before (Supplementary Fig. 1).

These results suggest that synaptic interference of rivastigmine with the pharmacological activity of HMTM – reflected as differential abundance of selected synaptic proteins in the COMB-15/0.5 cohort – can be shown in the tau-overexpressing L1 mouse model and, to a lesser extent, in wild-type mice.

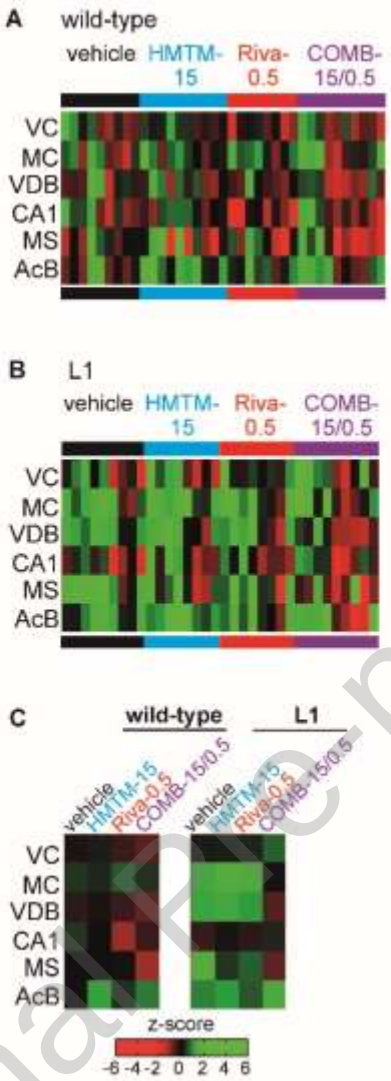

Fig. 4 Effect of the different treatments on average synaptic protein expression in L1 and wild-type mice. The abundance (z-score) of all six synaptic proteins was averaged for each region of interest to visualise a region-specific expression pattern in wild-type (A) and L1 mice (B), treated with vehicle, HMTM-15, Riva-0.5 or their combination (COMB-15/0.5). The group medians for each of these treatments are shown for each genotype (C).

Effect of HMTM, Riva and their combination on SNARE and non-SNARE proteins

Next, protein- and region-specific expression patterns (heat maps and estimation plots) for SNARE (Fig. 5-6) and non-SNARE (Fig. 7-8) proteins were created.

We first explored the expression patterns of the SNARE proteins SNTX-1, SNAP-25, and VAMP-2. In wild-type mice (Fig. 5A), HMTM-15 decreased expression of the three SNARE proteins in VC/MC. Riva-0.5 decreased SNARE expression in VC/MC and additionally in CA1. COMB-15/0.5 showed similar effects to Riva-0.5 alone in VC/CA1, but in MC protein expression was reversed to vehicle-treated levels. In L1 mice (Fig. 5B), the effect of the drugs was mixed; for example, expression was unaffected in MS/AcB with HMTM-15 and Riva-0.5 compared to vehicle-treated L1 but was globally decreased with COMB-15/0.5 treatment in most areas. Overall, when group medians were plotted (Fig. 5C), HMTM-15 had subtle effects on protein expression. By contrast, Riva-0.5 led to a significant reduction of cortex proteins (VC/MC/CA1; $F(1, 270) = 11.38$; $p = 0.0009$). This effect was reiterated by COMB-15/0.5 ($F(1, 288) = 11.31$; $p = 0.0009$). In L1 mice, SNARE protein abundance was significantly heightened in basal forebrain and lowered in cortex (main effect of genotype $F(1, 288) = 5.88$; $p = 0.016$). While HMTM-15 globally heightened SNARE protein expression this was not found with Riva-0.5, and the combination of both drugs (COMB-15/0.5) caused yet a greater decrease in global expression.

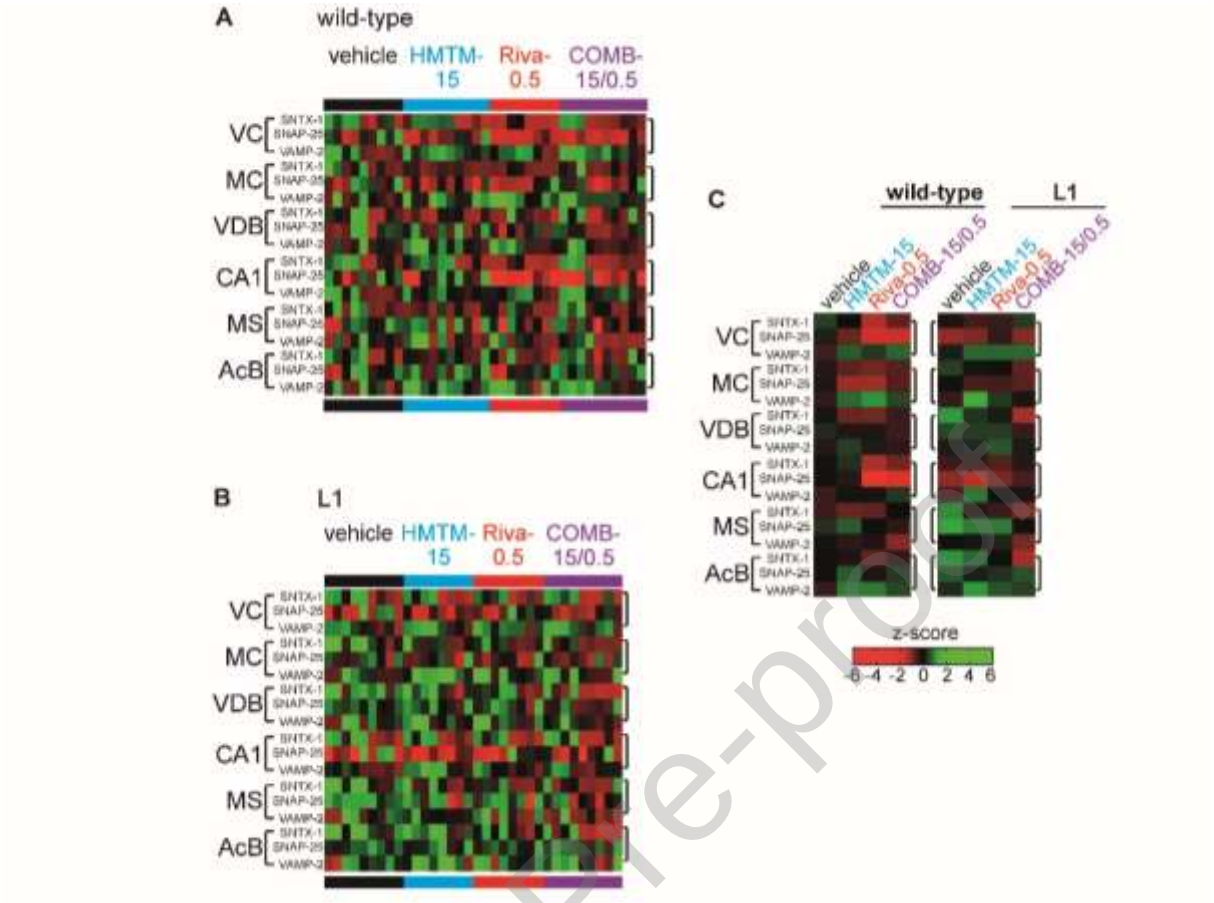

Fig. 5 Treatment heatmaps for SNARE proteins in L1 and wild-type mice. To visualise expression patterns for SNARE proteins, individual protein abundances (z-scores) are shown for the SNARE proteins SNTX-1, SNAP-25 and VAMP-2 as expression heatmaps organised by region of interest in wild-type (A) and L1 mice (B), as well as for each genotype, where the group median is shown for each protein and each treatment (C).

Estimation plots for wild-type mice, showed that SNTX-1 (Supplementary Fig. 2A) was significantly reduced following HMTM-15 (Difference δ = -0.37, p = 0.038), Riva-0.5 (δ = -0.73, p = 0.002) and COMB-15/0.5 (δ = -0.21, p = 0.027). L1 mice had a significantly greater SNTX-1 protein abundance over all areas when compared to vehicle-treated wild-type mice (δ = 0.63, p = 0.018) and this was corrected to wild-type levels when L1 (Fig. 6A) were treated with HMTM-15 (δ = 0.19, p: ns) or Riva-0.5 (δ = -0.14, p: ns), but decreased much below the levels for wild-type with COMB-15/0.5 (δ = -0.33, p = 0.008). The corrective effect for HMTM when given alone was dose-dependent and this correction did not occur in the HMTM-5 cohort (δ = 0.31, p = 0.016, Supplementary Fig. 3A). The negative impact of COMB-15/0.5 (δ = -0.33, p = 0.008, see above), that reduced SNTX-1 much below wild-type levels, appeared to depend on the dosing as it was not seen in low-Riva in COMB-15/0.1 (δ = 0.35, p: ns) and depended on the higher dose of HMTM (COMB-5/0.1, δ = -0.24, p = 0.049).

SNAP-25 levels in wild-type mice (Supplementary Fig. 2B) remained unchanged following HMTM-15 (δ = -0.19, p: ns) but was significantly reduced following, Riva-0.5 (δ = -0.92, p = 0.03) and COMB-15/0.5 (δ = -0.70, p = 0.045). In L1 mice the abundance of SNAP-25 over all areas (Fig. 6B) did not differ significantly from vehicle-treated wild-type mice (δ = 0.14, ns), and none of the treatments in the core groups had any effect (δ = -0.27 for HMTM-15; δ = -0.07 for Riva-0.5 and δ = -0.30 for COMB-15/0.5, all p's = ns).

In wild-type mice, VAMP-2 (Supplementary Fig. 2C) was significantly elevated following HMTM-15 (δ = 0.57, p = 0.005), but not significantly changed with Riva-0.5 (δ = 0.49, ns) or COMB-15/0.5 (δ = 0.36, ns). In L1 mice VAMP-2 protein abundance over all areas (Fig. 6C) did not differ significantly from vehicle treated wild-type mice (δ = 0.10, ns). Treatment with HMTM-15 and Riva-0.5 but not COMB-15/0.5 significantly increased VAMP-2 in L1 cohorts (δ = 0.75, p = 0.01 for HMTM-15; δ = 0.52, p = 0.01 for Riva-0.5 and δ = 0.30, ns for COMB-15/0.5). The increase with HMTM was also achieved by the lower dose HMTM-5 (δ = 0.43, p = 0.003) but the Riva effect is dose dependent and was not seen with the lower dose Riva-0.1 (δ = 0.09, ns). All other COMB-treatments wiped out the HMTM increase (Supplementary Fig. 3C).

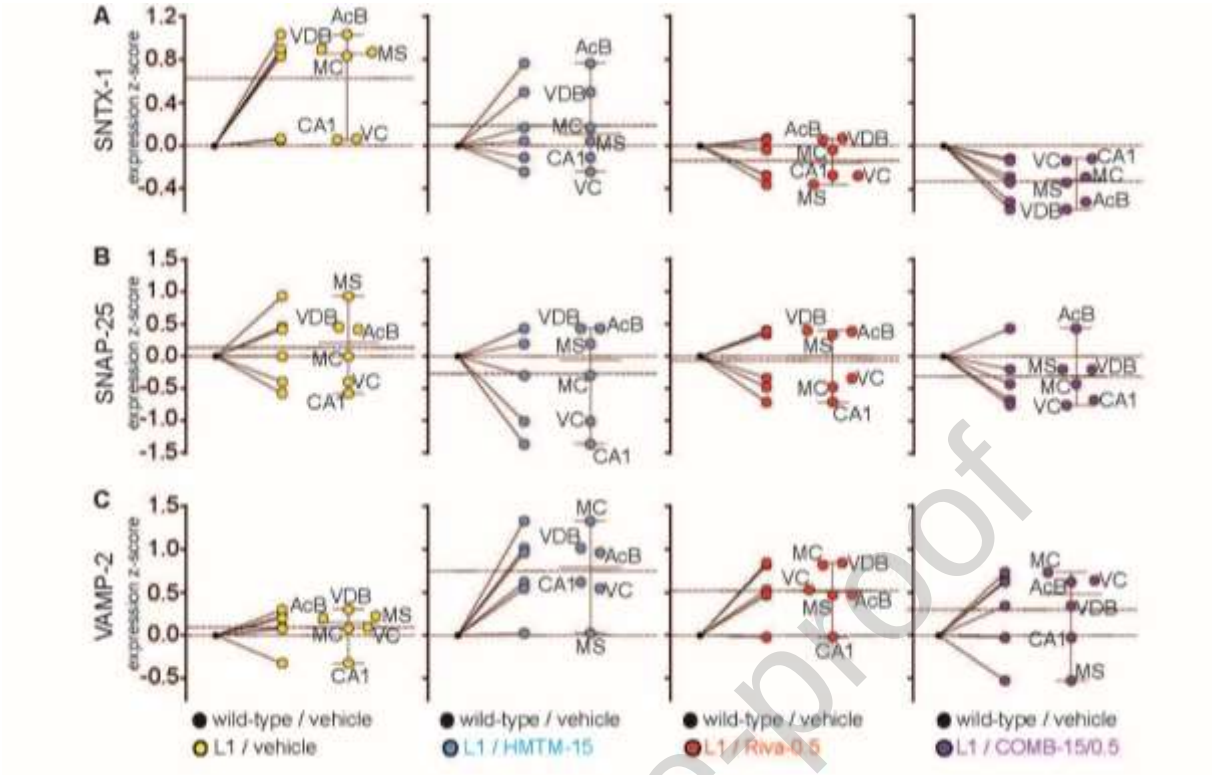

Fig. 6 Estimation of treatment effects on SNARE proteins in L1 mice. To visualise treatment effects on SNARE proteins in L1 mice, estimation plots are shown for the SNARE proteins SNTX-1 (A), SNAP-25 (B) and VAMP-2 (C), under vehicle (first column from left, yellow circles), HMTM-15 (second column from left, blue circles), Riva-0.5 (third column from left, red circles), and their combination COMB-15/0.5 (right column, purple circles), all compared to vehicle-treated wild-type mice (black symbol set to 0) in the 6 different regions VC, MC, VDB, CA1, MS, and AcB. Additionally, the average genotype/treatment effect is shown as a scatter plot on the right-hand side (median and 95% confidence interval) for each panel.

For the non-SNARE proteins SYNPY-1, SYN-1 and A-SYN, the effect of the drugs was more subtle than for the SNARE proteins, but there was a decrease of protein abundance in VDB/CA1/MS from wild-type mice following COMB-15/0.5 treatment, which was not seen when individual drugs HMTM-15 or Riva-0.5 were administered (Fig. 7A). Similar effects were observed in L1 mice in VDB/CA1/MS/AcB (Fig. 7B), however individual treatments led to a weak increase of global abundance of non-SNARE proteins. As with the SNARE proteins, this increase was converted to a reduction by COMB-15/0.5 (Fig. 7C).

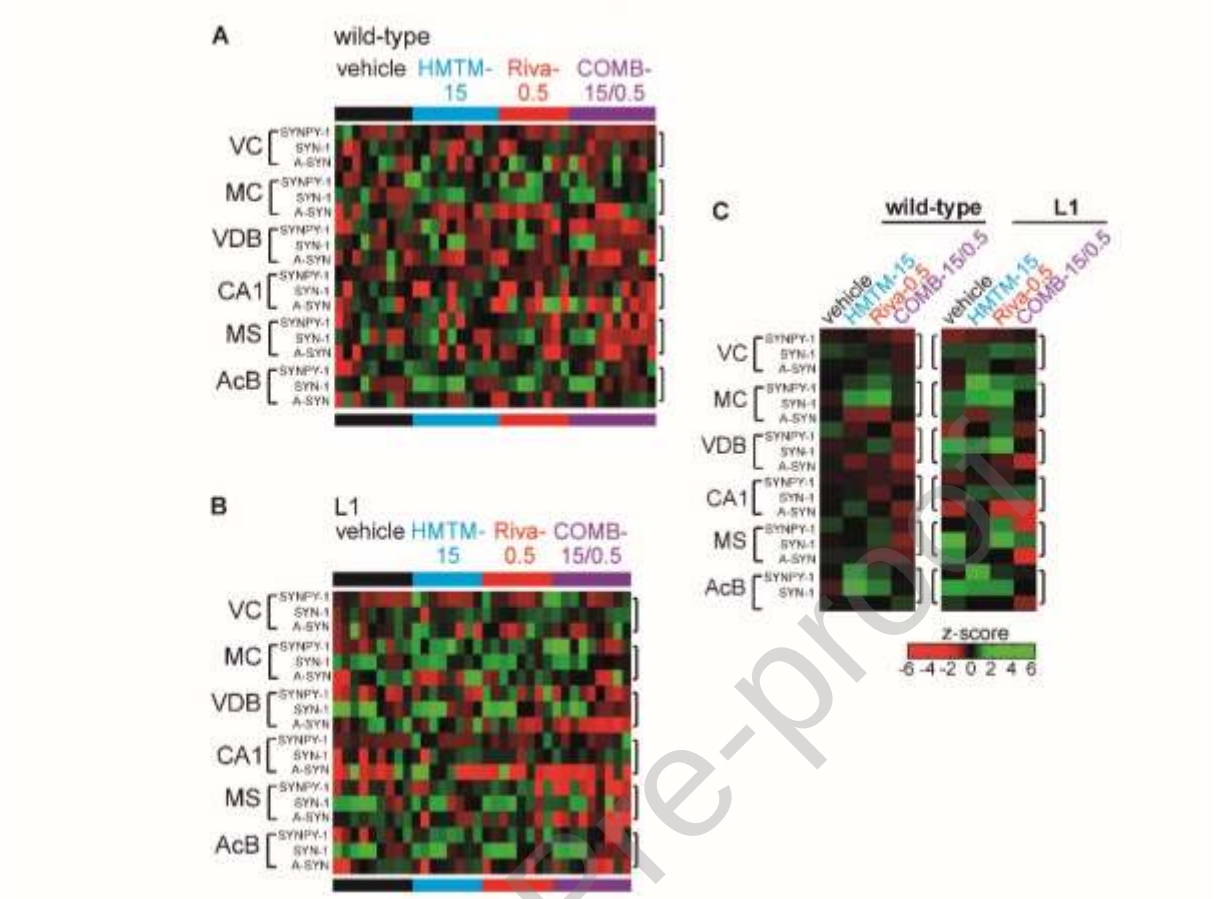

Fig. 7 Treatment heatmaps for non-SNARE proteins in L1 and wild-type mice. To visualise expression patterns for non-SNARE proteins, individual protein abundances (z-scores) are shown for SYNPY-1, SYN-1 and A-SYN as expression heatmaps organised by region of interest in wild-type (A) and L1 mice (B), as well as for each genotype, where the group median is shown for each protein and each treatment (C).

Estimation plots for the three non-SNARE protein abundance z-scores following the different drug treatments are depicted for wild-type in Supplementary Fig. 2D-F and L1 mice in Fig. 8. Again, the vehicle-treated wild-type mice were used as reference for all other groups (black symbol).

In wild-type mice, estimation plots revealed no significant protein z-score changes for any of the non-SNARE proteins SYNPY-1, SYN-1 and A-SYN following treatment with HMTM-15, Riva-0.5 or COMB-15/0.5 (Supplementary Fig. 2D-F).

In L1 mice, abundance of SYNPY-1 over all areas (Fig. 8A) was significantly reduced when compared to vehicle-treated wild-type mice ($\delta = -0.39$, $p = 0.014$). This was normalised to wild-type levels when mice were treated with HMTM-15 ($\delta = 0.41$, ns), Riva-0.5 ($\delta = 0.37$, ns) and COMB-15/0.5 ($\delta = 0.01$, ns). The same effect was achieved with the lower dose of HMTM-5 ($\delta = 0.01$, ns), but not the lower dose of Riva-0.1 alone ($\delta = -0.44$, $p = 0.036$) or combined (COMB-5/0.1, $\delta = -0.77$, $p = 0.041$). This negative effect was overcome by the dominant effect of the higher dose of HMTM (COMB-15/0.1, $\delta = 0.38$, ns; Supplementary Fig. 3D). SYN-1 in L1 (Fig. 8B) was significantly elevated when compared to vehicle-treated wild-type mice ($\delta = 0.75$, $p = 0.048$) and was not corrected by either treatment ($\delta = 0.71$, $p = 0.005$ for HMTM-15; $\delta = 0.98$, $p = 0.003$ for Riva-0.5 and $\delta = 0.97$, $p = 0.012$ for COMB-15/0.5). A-SYN in L1 (Fig. 8C) was significantly increased when compared to vehicle-treated wild-type mice ($\delta = 0.35$, $p = 0.041$), corrected by HMTM-15 ($\delta = 0.09$, ns) and Riva-0.5 ($\delta = 0.13$, ns), but decreased below wild-type levels with COMB-15/0.5 ($\delta = -0.72$, $p = 0.06$). This negative interaction was dependent on the high dose of Riva-0.5 and not seen at the lower dose ($\delta = -0.73$, ns for COMB-5/0.1 and $\delta = -0.04$, ns for COMB-15/0.1; Supplementary Fig. 3F).

Taken together, these results suggest a normalisation of synaptic protein abundance following treatment with HMTM in the tau-transgenic L1 mouse model, e.g., SNTX-1, SYNPY-1, and A-SYN. There was a wide-spread negative interference with the efficacy of HMTM by co-treatment with rivastigmine. This inhibitory effect of rivastigmine on HMTM-related synaptic protein normalisation was less prominent when the lower dose of rivastigmine was used for pre-treatment.

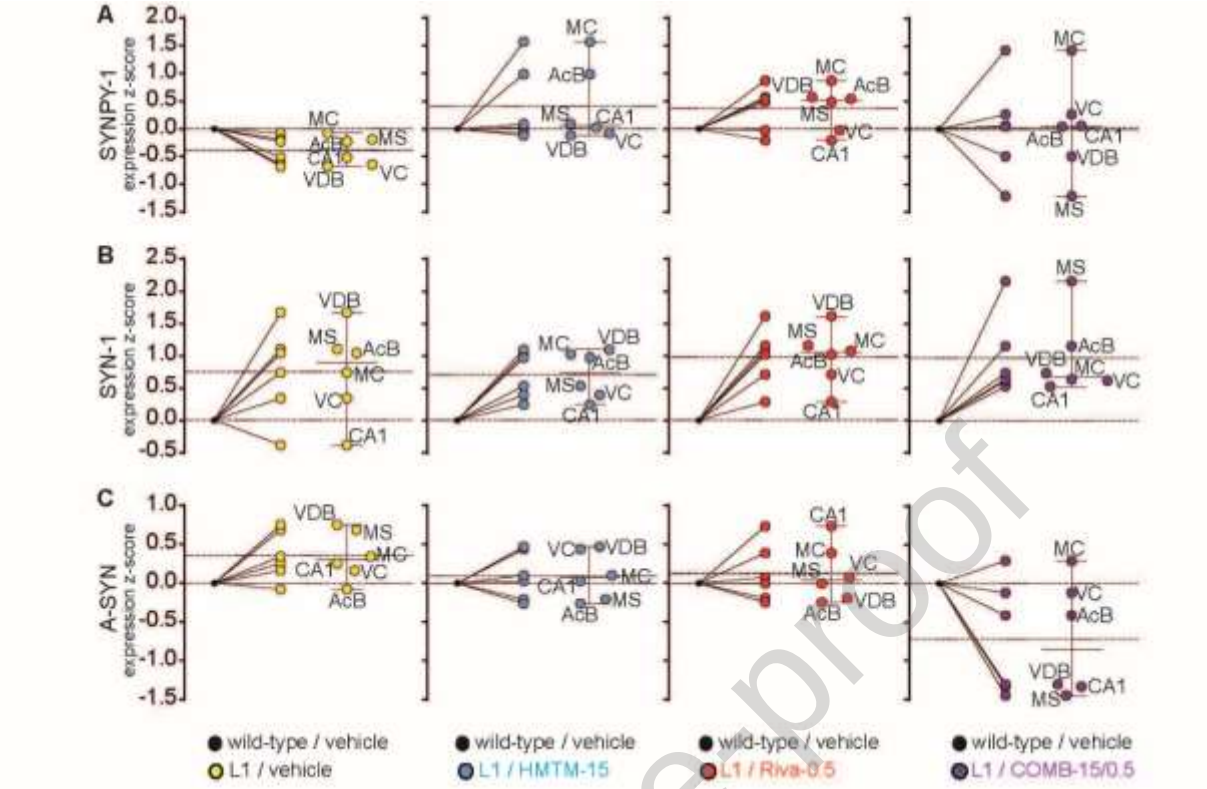

Fig. 8 Estimation of treatment effects on non-SNARE proteins in L1 mice. To visualise treatment effects on non-SNARE proteins in L1 mice, estimation plots are shown for SYNPY-1 (A), SYN-1 (B) and A-SYN (C), under vehicle (first column from left, yellow circles), HMTM-15 (second column from left, blue circles), Riva-0.5 (third column from left, red circles), and their combination COMB-15/0.5 (right column, purple circles), all compared to vehicle-treated wild-type mice (black symbols) in the 6 different regions VC, MC, VDB, CA1, MS, and AcB. Additionally, the average genotype/treatment effect is shown as a scatter plot on the right-hand side (median and 95% confidence interval) for each panel.

Correlation of SNARE and non-SNARE proteins is different between genotypes and affected by drugs in a brain region-specific manner

Group-based, pair-wise correlation matrices were created using Pearson´s correlation for wild-type and L1 mice and the effect of the different drugs in the core groups (vehicle, HMTM-15, Riva-0.5 and COMB-15/0.5) on the six synaptic proteins was assessed and clustered by brain regions (Fig. 9A). Co-expression relationships (positive correlation coefficients) are blue, while inverse expression relationships (negative correlation coefficients) are shown in yellow in the correlation matrix and *p*-values for statistically significant correlations are purple (Fig. 9B). The maps show prominent differences between both genotypes and treatments.

Highlighted in black squares are correlations between basal forebrain regions (MS, VBD and AcB). There was a minor increase in negative (yellow) correlations between vehicle-treated L1 and wild-type cohorts. Furthermore, relative to wild-type controls, more positive (blue) correlations emerged in groups administered with HMTM or COMB-15/0.5. In L1 mice, the most prominent increases were observed for treatments of rivastigmine and COMB-15/0.5. This distinction suggests heightened sensitivity to rivastigmine in L1 mice possibly due to cholinergic deficiencies.

The red squares highlight the correlations between the basal forebrain and cortex. These become more positive in L1 (vehicle) compared to wild-type. Negligible effect in wild-type mice was seen with monotherapy but a prominent increase in positive correlations was achieved following COMB-15/0.5 treatment. By contrast, both HMTM and rivastigmine increased positivity of correlations in L1 (HMTM between CA1/VC vs. MS/VDB, and rivastigmine between MC vs. MS/VDB/AcB). Intriguingly, COMB-15/0.5 treatment in L1 heightened negative correlations. For intracortical correlations, there is therefore a negative interference between the two treatments, most prominent in L1 mice.

These results confirm the differential actions of HMTM on synaptic protein correlations either when given alone or when given as add-on to mice pre-treated with rivastigmine.

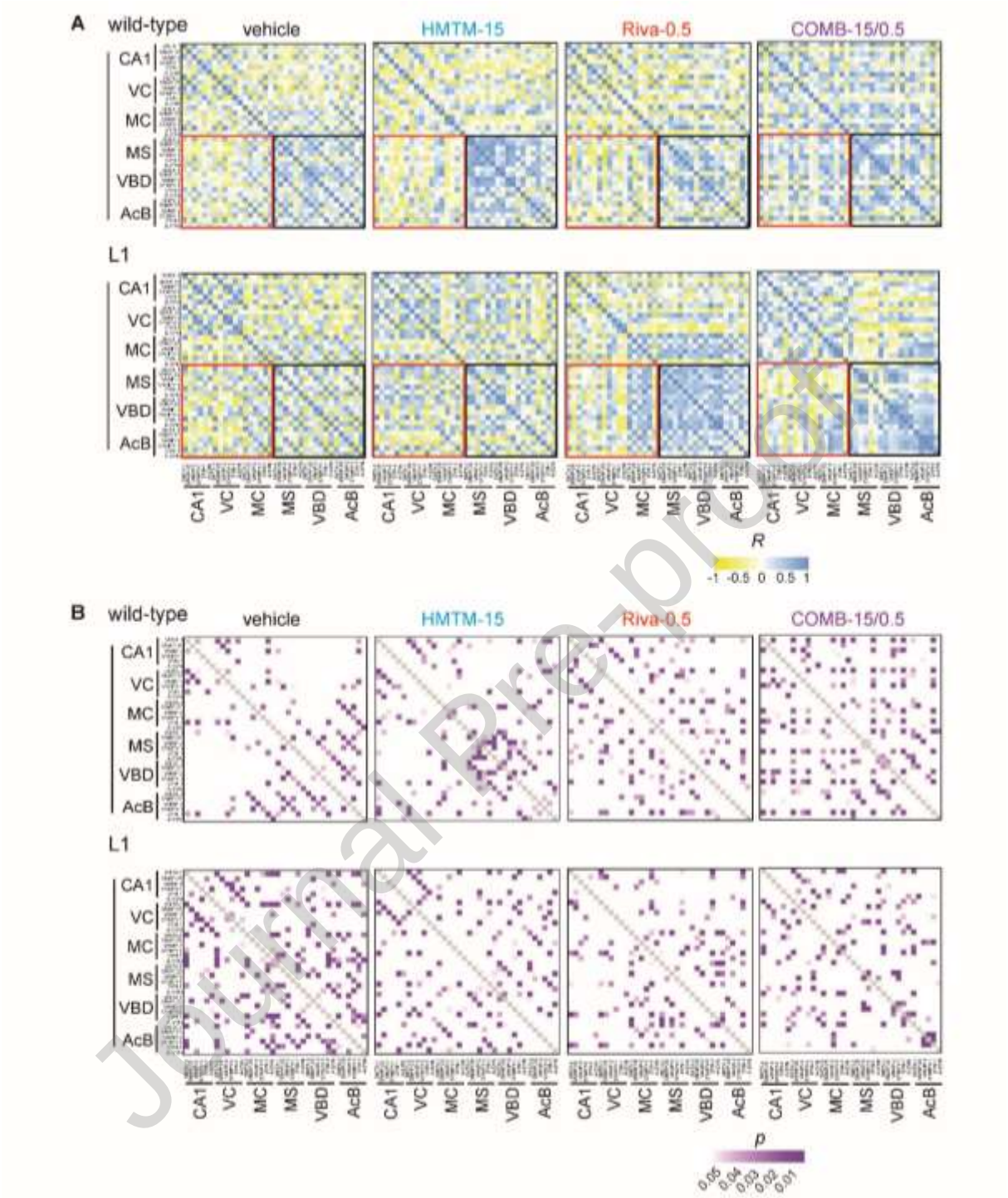

Fig. 9 Effect of the different treatments on correlation of SNARE and non-SNARE protein abundance in L1 and wild-type mice. Pearson's correlations (R) and the resulting *p*-values are shown as correlation heatmaps for wild-type and L1 mice. The protein correlations are shown for the six proteins SNTX-1, SNAP-25, VAMP-2, SYNPY-1, SYN-1, and A-SYN clustered by region (A). Positive correlations are blue, inverse correlations are yellow, if correlation is lacking (R close to 0) then cells are labelled in white. Corresponding *p*-values are coloured purple, lack of significancy is shown in white (B). The black squares highlight protein correlations within the basal forebrain (MS, VDB and AcB) while the red squares highlight protein correlations between the basal forebrain and the cortex (CA1, VC and MC).

Discussion

In two large clinical trials for mild and mild/moderate AD (NCT01689233 and NCT01689246, respectively), HMTM failed to show the same efficacy when administered as an add-on to ongoing symptomatic treatment with AChEI (e.g., rivastigmine, donepezil or galantamine) and / or the NMDA receptor antagonist memantine, while it produced significant arrest of cognitive and functional decline in subjects receiving the drug as monotherapy *(26, 27)*. This reduction in pharmacological activity of HMTM when given as an add-on was also reproduced in a tau transgenic mouse model L1, in which chronic pre-treatment with the AChEI rivastigmine blunted the pharmacological efficacy of HMTM at multiple brain systems including hippocampal acetylcholine levels, behavioural performance in the water maze, synaptosomal glutamate release and mitochondrial activity (summarised in *(24)*). Alterations in neurotransmitter release might be explained by changes in the synaptic structure or function, both of which can be deduced from the proteins analysed here.

In the current study, we examined the levels of synaptic proteins following treatment with HMTM either administered singly or given as an add-on to rivastigmine. The key findings that we report are that:

(i) for L1 tau-transgenic mice, levels of synaptic proteins were reduced in cortex, but heightened in the basal forebrain relative to wild-type mice.
(ii) protein levels in wild-type cohorts were most altered in rivastigmine cohorts (single and combination treatment).
(iii) HMTM in L1 normalised the expression pattern of SNTX-1/A-SYN in basal forebrain; and
(iv) HMTM combined with rivastigmine in L1 led to a large decrease in these synaptic proteins, well below wild-type levels.

From these data, we determined correlations between proteins and regions and confirmed that:

(i) anomalies for intra- (basal forebrain) and extra-regional (basal forebrain to cortex) protein correlations in L1.
(ii) normalisation of correlations most prominently for SNARE proteins in L1 treated with HMTM; and
(iii) heightened positive correlations induced by HMTM were lost by pre-treatment with rivastigmine.

Levels of synaptic proteins in neurodegeneration

Motor and cognitive impairments in many neurodegenerative disorders such as AD are associated with structural synapse alterations (for review see *(35)*). These alterations involve thousands of proteins constituting the synaptic machinery with highly complex biological and signalling properties *(54–57)*. It is intuitively clear that the lifetime of both structural (such as tau protein) and functional proteins (for instance SNARE proteins) is critical for synapse maintenance, remodelling and ageing. Especially for cortical and hippocampal synapses, the lifetime synaptome atlas has shown that short-lived proteins are enriched in young subjects, while during ageing, proteins with long lifetimes are enriched in the synapse *(58)*. Since a reduction of presynaptic proteins in cortex and hippocampus in AD is consistently reported *(59)*, and confirmed here in this study for our tau mouse model, it is in particular the proteins with a normally long lifetime that are decaying in L1. However, these are not readily regenerated in aged subjects and under tau oligomerisation. We hypothesise that both abundance and thus function of synapse proteins are rescued in L1 with HMTM treatment. By contrast, combined administration of rivastigmine and HMTM led to a further reduction in synaptic protein levels (see Fig. 4C&5C contrasting HMTM versus HMTM + rivastigmine). Such an action would be considered detrimental for the cortical/hippocampal network and its function such as memory formation, recall of stored information, and learning.

L1 mice overexpress tau297-391, the truncated repeat domain of tau that corresponds to the core fragment of PHF-tau found in AD brain tissue. The mice present with neuroanatomical spread of pathological tau with age that results in cognitive decline, cholinergic loss in basal forebrain, and altered brain bioenergetics *(12, 45, 60)*. Additionally, we show here that the core fragment of tau in L1 is present and accumulates in multiple brain regions and. most likely, in the presynaptic compartment (as reported for another transgenic tau mouse, Line 66 *(61)*). Especially in hippocampus and cortex, this may lead directly to a reduction of synaptic proteins in L1. Reduction of pre-synaptic proteins in AD brains occurs prominently in hippocampus and frontal cortex, mainly for syntaxin-1, SNAP-25, and VAMP-2, synaptophysin-1, and synapsin-1, while in basal forebrain rather post-synaptic markers such as Ras GTPase-activating protein (downstream effector of e.g. glutamate receptors) are reduced *(59)*. The interactions between syntaxin-1, SNAP-25, and VAMP-2 and synapsin/synaptophysin, are crucial for the formation of synaptic vesicles and their quantal release in response to incoming electrophysiological discharges *(37, 62)*. Although no direct protein interaction experiments between tau and other synaptic proteins were attempted here, the binding of truncated tau to transmembrane proteins is likely to interfere with the formation of synaptic vesicles in general and the SNARE complex assembly in particular *(63–65)*, as shown in this study for L1 mice.

It is conceivable that heightened expression of presynaptic proteins in basal forebrain of L1 is likely due to strengthened afferents compensating for cholinergic loss. Heightened presynaptic protein levels, and thus increased number of synapses, could arise from a multitude of connections with high contents of glutamatergic *(66, 67)*, GABAergic *(68, 69)*, and serotonergic origin *(70)*. While these have not been differentiated in this study, this may be interpreted as an attempt by the brain to increase tonic activity of basal forebrain centres, and potentially correct for decreased acetylcholine release in target structures such as hippocampus or prefrontal cortex *(45, 71, 72)*. Functionally, such a neurophysiological trait residing in basal forebrain of L1, may be considered a noisy brain state with the potential to limit memory formation by way of signal suppression due to uncoordinated synaptic hyper-activity *(73–75)*. HMTM may therefore not only have corrected levels of synaptic proteins exemplified by SNTX-1 or A-SYN but may also have improved physiological fingerprints of synaptic function/neurotransmitter release. In this way, HMTM may directly recover cholinergic function *(49)* as well as cognition in L1 mice *(12)*. That rivastigmine given at therapeutically relevant doses was unable to correct the change in expression of synaptic proteins in cortex/basal forebrain is due to its pharmacologically different profile and mode of action. HMTM has strong tau aggregation inhibition activity (*(8, 9)*; yet rivastigmine is a selective cholinesterase inhibitor which does not appear to correct mechanistic modifications at the synaptic level and does not seem to rescue cognitive function in mild cognitive impairment *(76, 77)*. Quite the opposite, the long-term pre-exposure reduces the sensitivity of synapses to HMTM. This is mechanistically unexplained by our data and would require a more detailed approach to distinguish drug action on the different transmitter systems and their synaptic connectome.

Correlations between synaptic proteins and brain structures

We have previously shown, by structural correlation network analysis, that an abnormal increase in correlations occurs in AD relative to healthy elderly control subjects for functionally connected brain areas *(33)*. We suspect these structural correlations to be mediated, at least in part, by variable expression of synaptic proteins. For example, a significant decline in levels of the SNARE protein SNAP-25 was recorded in AD brains by Bereczki and colleagues *(78)* and later confirmed by others *(79, 80)*. Moreover, the lowering of SNAP-25 in cortex of patients was associated with the rate of cognitive decline confirming the importance of synaptic integrity for memory formation. A similar network analysis was conducted for L1 mice with the aim to determine whether synaptic protein levels correlate intrinsically or extrinsically within or between regions of interest. Globally, cortical structures were contrasted with basal forebrain regions. The network analysis established abnormal co-expression correlations of

SNARE proteins within basal forebrain or long-distance between basal forebrain and cortex in L1, and these were modulated by HMTM. However, similar modifications were not observed in the groups treated with rivastigmine or rivastigmine/HMTM combinations strongly suggesting that pre-exposure to AChEIs prevents the synaptic benefit offered by HMTM.

A recent study confirmed a direct correlation between dysregulation of SNARE proteins and cognitive decline *(81)*. Similar alterations in SNARE correlations are reported here for our L1 model. These alterations may indeed be due to the accumulation of tau, since the abundance of several synaptic proteins changes with advancing Braak stage of neuropathology in AD *(82)*. Again, synaptic expression of tau is likely to interfere prominently with SNARE complex assembly *(61, 63, 65, 83)*, and this would explain the loss of correlation of SNARE protein co-expression observed in L1 mice. Tau accumulation in L1 is also held responsible for the reduction in cholinergic neurons in basal forebrain and hippocampal acetylcholine levels, and these can indeed be rescued by the treatment with HMTM *(24)*.

Dynamic modulation of HMTM effects by prior exposure to cholinesterase inhibition

Although this work confirms that the expression of the tau core domain in synaptic structures in all regions of interest, a more quantitative analysis has shown a strong reduction of this immunoreactivity in the presence of HMTM *(24)*. Our approach did not allow differentiation of origins of input for the presynaptic structures examined here, or transmitters released at individual synapses (see above). However, it is likely that specific subpopulations of afferents are differentially sensitive to tau-toxicity and glutamatergic and cholinergic synapses seem particularly vulnerable and sensitive to HMTM treatment *(49)*. Importantly, we have also shown that the negative impact of the combination treatment on synaptic protein levels/correlations was not readily overcome by reducing the dose of rivastigmine and/or increasing the dose of HMTM (e.g., VAMP-2 and SYNPY-1 but not the other proteins) suggesting that chronic pre-treatment with AChEIs may lead to irreversible homeostatic adjustments in the physiology of the demented brain and our correlation analysis supports this notion. The only HMTM-treatment effect that is not subject to pharmacological interference is the primary effect on tau aggregation pathology *(24)*. Recent failures of trials for novel therapies of AD administered on the background of symptomatic treatment seem to corroborate this hypothesis *(7)*. Thus, the assumption that symptomatic treatment does not interfere with disease-modifying therapy might need revision *(24)*.

In summary, we have shown that several HMTM effects can be modulated by the prior administration with the AChEI rivastigmine and these include increase in hippocampal acetylcholine release/mitochondrial complex IV activity, reversal of behavioural impairment *(24)* and, in this study, abnormal increase/decrease of levels and network correlations of synaptic proteins.

Abbreviations

AcB: nucleus accumbens; AChEI: acetylcholinesterase inhibitors; AD: Alzheimer´s disease; A-SYN: alpha-synuclein; CA1: hippocampal CA1 region; HMTM: N3,N3,N7,N7-tetramethyl-10*H*-phenothiazine-3,7-diaminium bis (methanesulfonate) (leuco-methylthioninium bis(hydromethanesulfonate); MC: primary motor cortex; MS: medial septum; MT: methylthioninium; MTC: methylthioninium chloride; SNAP-25: synaptosomal-associated protein 25; SNARE: Soluble N-ethylmaleimide-sensitive factor attachment protein receptor; SNTX-1: syntaxin-1; SYN-1: synapsin-1; SYNPY-1: synaptophysin-1; VAMP-2: vesicle-associated membrane protein 2; VC: visual cortex ; VDB: vertical limb of the diagonal band of Broca.

Institutional Review Board Statement

All animal experiments were performed in accordance with the European Communities Council Directive (63/2010/EU) and a project licence with local ethical approval under the Polish Law on the Protection of Animals and National Institute of Health's Guide for Care and Use of Laboratory Animals (Publication No. 85-23, revised 1985) and comply with the ARRIVE guidelines 2.0. No human tissues were used in this study.

Availability of data and materials

All data are provided within the manuscript or the Supporting data file.

Conflicts of interest

C.R.H. and C.M.W. declare that they are officers in TauRx Therapeutics Ltd. K.S., C.R.H., C.M.W. and G.R. are named inventors on patent applications relating to HMTM and tau protein.

Funding

This work was funded by WisTa Laboratories Ltd., an affiliate of TauRx Therapeutics Ltd., Singapore (PAR1562 and PAR1763).

Author Contributions

KS: Conceptualization, Methodology, Formal analysis, Investigation, Data Curation, Visualization, Writing - Original Draft, Writing - Review & Editing; DL: Investigation, Data Curation, Formal analysis; MM: Investigation; FT: Supervision, Project administration, Funding acquisition; AG: Investigation; MZ: Investigation; CRH: Conceptualization, Funding acquisition, Writing - Review & Editing; CMW: Funding acquisition, Writing - Review & Editing; GN: Supervision, Project administration, Funding acquisition, Resources; GR: Conceptualization, Supervision, Writing - Review & Editing.

Author Statement

All authors have seen and agreed with this manuscript and their individual contributions are listed below (and as part of the manuscript).

KS: Conceptualization, Methodology, Formal analysis, Investigation, Data Curation, Visualization, Writing - Original Draft, Writing - Review & Editing; DL: Investigation, Data Curation, Formal analysis; MM: Investigation; FT: Supervision, Project administration, Funding acquisition; AG: Investigation; MZ: Investigation; CRH: Conceptualization, Funding acquisition, Writing - Review & Editing; CMW: Funding acquisition, Writing - Review & Editing; GN: Supervision, Project administration, Funding acquisition, Resources; GR: Conceptualization, Supervision, Writing - Review & Editing.

Declaration of interest

C.R.H. and C.M.W. declare that they are officers in TauRx Therapeutics Ltd. K.S., C.R.H., C.M.W. and G.R. are named inventors on patent applications relating to HMTM and tau protein.

Acknowledgements

The authors acknowledge Malgorzata Wydrych and Joanna Lewandowska for the technical support with perfusion of mice and collection of brains, and of Soumya Palliyil Soman for the development of the s1D12 antibody.

References

1. S. M. Li, M. S. Mo, P. Y. Xu, Progress in mechanisms of acetylcholinesterase inhibitors and memantine for the treatment of Alzheimer's disease. *Neuroimmunol. Neuroinflammation* **2**, 274–280 (2015).

2. J. Ferrero, L. Williams, H. Stella, K. Leitermann, A. Mikulskis, J. O'Gorman, J. Sevigny, First-in-human, double-blind, placebo-controlled, single-dose escalation study of aducanumab (BIIB037) in mild-to-moderate Alzheimer's disease. *Alzheimer's Dement. Transl. Res. Clin. Interv.* **2**, 169–176 (2016).

3. J. Sevigny, P. Chiao, T. Bussière, P. H. Weinreb, L. Williams, M. Maier, R. Dunstan, S. Salloway, T. Chen, Y. Ling, J. O'Gorman, F. Qian, M. Arastu, M. Li, S. Chollate, M. S. Brennan, O. Quintero-

Monzon, R. H. Scannevin, H. M. Arnold, T. Engber, K. Rhodes, J. Ferrero, Y. Hang, A. Mikulskis, J. Grimm, C. Hock, R. M. Nitsch, A. Sandrock, The antibody aducanumab reduces Aβ plaques in Alzheimer's disease. *Nature* **537**, 50–56 (2016).

4. D. S. Knopman, D. T. Jones, M. D. Greicius, Failure to demonstrate efficacy of aducanumab: An analysis of the EMERGE and ENGAGE trials as reported by Biogen, December 2019. *Alzheimer's Dement.* **17**, 696–701 (2021).

5. M. Tolar, S. Abushakra, J. A. Hey, A. Porsteinsson, M. Sabbagh, Aducanumab, gantenerumab, BAN2401, and ALZ-801 - The first wave of amyloid-targeting drugs for Alzheimer's disease with potential for near term approval. *Alzheimer's Res. Ther.* **12**, 1–10 (2020).

6. S. C. C.H. van Dyck, C.J. Swanson, P. Aisen, R.J. Bateman, C. Chen, M. Gee, M. Kanekiyo, D. Li, L. Reyderman, and T. I. L. Froelich, S. Katayama, M. Sabbagh, B. Vellas, D. Watson, S. Dhadda, M. Irizarry, L.D. Kramer, Lecanemab in Early Alzheimer's Disease. *N. Engl. J. Med.* **388**, 9–21 (2023).

7. J. L. Cummings, G. Tong, C. Ballard, Treatment Combinations for Alzheimer's Disease: Current and Future Pharmacotherapy Options. *J. Alzheimer's Dis.* **67**, 779–794 (2019).

8. C. R. Harrington, J. M. D. Storey, S. Clunas, K. A. Harrington, D. Horsley, A. Ishaq, S. J. Kemp, C. P. Larch, C. Marshall, S. L. Nicoll, J. E. Rickard, M. Simpson, J. P. Sinclair, L. J. Storey, C. M. Wischik, Cellular models of aggregation-dependent template-directed proteolysis to characterize Tau aggregation inhibitors for treatment of Alzheimer disease. *J. Biol. Chem.* **290**, 10862–10875 (2015).

9. Y. K. Al-Hilaly, S. J. Pollack, J. E. Rickard, M. Simpson, A. C. Raulin, T. Baddeley, P. Schellenberger, J. M. D. Storey, C. R. Harrington, C. M. Wischik, L. C. Serpell, Cysteine-Independent Inhibition of Alzheimer's Disease-like Paired Helical Filament Assembly by Leuco-Methylthioninium (LMT). *J. Mol. Biol.* **430**, 4119–4131 (2018).

10. E. E. Congdon, J. W. Wu, N. Myeku, Y. H. Figueroa, M. Herman, P. S. Marinec, J. E. Gestwicki, C. A. Dickey, W. H. Yu, K. E. Duff, Methylthioninium chloride (methylene blue) induces autophagy and attenuates tauopathy in vitro and in vivo. *Autophagy* **8**, 609–622 (2012).

11. M. Hosokawa, T. Arai, M. Masuda-Suzukake, T. Nonaka, M. Yamashita, H. Akiyama, M. Hasegawa, Methylene Blue Reduced Abnormal Tau Accumulation in P301L Tau Transgenic Mice. *PLoS One* **7** (2012), doi:10.1371/journal.pone.0052389.

12. V. Melis, M. Magbagbeolu, J. E. Rickard, D. Horsley, K. Davidson, K. A. Harrington, K. Goatman, E. A. Goatman, S. Deiana, S. P. Close, C. Zabke, K. Stamer, S. Dietze, K. Schwab, J. M. D. Storey, C. R. Harrington, C. M. Wischik, F. Theuring, G. Riedel, Effects of oxidized and reduced forms of methylthioninium in two transgenic mouse tauopathy models. *Behav. Pharmacol.* **26**, 353–368 (2015).

13. T. C. Baddeley, J. McCaffrey, J. M. D. Storey, J. K. S. Cheung, V. Melis, D. Horsley, C. R. Harrington, C. M. Wischik, Complex disposition of methylthioninium redox forms determines efficacy in tau aggregation inhibitor therapy for Alzheimer's disease. *J. Pharmacol. Exp. Ther.* **352**, 110–118 (2015).

14. C. M. Wischik, R. T. Staff, D. J. Wischik, P. Bentham, A. D. Murray, J. M. D. Storey, K. A. Kook, C. R. Harrington, Tau aggregation inhibitor therapy: An exploratory phase 2 study in mild or moderate Alzheimer's disease. *J. Alzheimer's Dis.* **44**, 705–720 (2015).

15. K. Hochgräfe, A. Sydow, D. Matenia, D. Cadinu, S. Könen, O. Petrova, M. Pickhardt, P. Goll, F. Morellini, E. Mandelkow, E. M. Mandelkow, Preventive methylene blue treatment preserves cognition in mice expressing full-length pro-aggregant human Tau. *Acta Neuropathol. Commun.* **3**, 25 (2015).

16. D. Tucker, Y. Lu, Q. Zhang, From Mitochondrial Function to Neuroprotection—an Emerging Role for Methylene Blue. *Mol. Neurobiol.* **55**, 5137–5153 (2018).

17. A. P. Gureev, M. Y. Syromyatnikov, T. M. Gorbacheva, A. A. Starkov, V. N. Popov, Methylene blue improves sensorimotor phenotype and decreases anxiety in parallel with activating brain mitochondria biogenesis in mid-age mice. *Neurosci. Res.* **113**, 19–27 (2016).

18. C. Stack, S. Jainuddin, C. Elipenahli, M. Gerges, N. Starkova, A. A. Starkov, M. Jové, M. Portero-

Otin, N. Launay, A. Pujol, N. A. Kaidery, B. Thomas, D. Tampellini, M. Flint Beal, M. Dumont, Methylene blue upregulates Nrf2/ARE genes and prevents tau-related neurotoxicity. *Hum. Mol. Genet.* **23**, 3716–3732 (2014).

19. M. Zhao, F. Liang, H. Xu, W. Yan, J. Zhang, Methylene blue exerts a neuroprotective effect against traumatic brain injury by promoting autophagy and inhibiting microglial activation. *Mol. Med. Rep.* **13**, 13–20 (2016).

20. Y. Wen, W. Li, E. C. Poteet, L. Xie, C. Tan, L. J. Yan, X. Ju, R. Liu, H. Qian, M. A. Marvin, M. S. Goldberg, H. She, Z. Mao, J. W. Simpkins, S. H. Yang, Alternative mitochondrial electron transfer as a novel strategy for neuroprotection. *J. Biol. Chem.* **286**, 16504–16515 (2011).

21. K. K. Lee, U. A. Boelsterli, Bypassing the compromised mitochondrial electron transport with methylene blue alleviates efavirenz/isoniazid-induced oxidant stress and mitochondria-mediated cell death in mouse hepatocytes. *Redox Biol.* **2**, 599–609 (2014).

22. H. Atamna, J. Mackey, J. M. Dhahbi, Mitochondrial pharmacology: Electron transport chain bypass as strategies to treat mitochondrial dysfunction. *BioFactors* **38**, 158–166 (2012).

23. H. Atamna, A. Nguyen, C. Schultz, K. Boyle, J. Newberry, H. Kato, B. N. Ames, Methylene blue delays cellular senescence and enhances key mitochondrial biochemical pathways. *FASEB J.* **22**, 703–712 (2008).

24. G. Riedel, J. Klein, G. Niewiadomska, C. Kondak, K. Schwab, D. Lauer, M. Magbagbeolu, M. Steczkowska, M. Zadrozny, M. Wydrych, A. Cranston, V. Melis, R. X. Santos, F. Theuring, C. R. Harrington, C. M. Wischik, Mechanisms of Anticholinesterase Interference with Tau Aggregation Inhibitor Activity in a Tau-Transgenic Mouse Model. *Curr. Alzheimer Res.* **17**, 285–296 (2020).

25. K. Schwab, V. Melis, C. R. Harrington, C. M. Wischik, M. Magbagbeolu, F. Theuring, G. Riedel, Proteomic Analysis of Hydromethylthionine in the Line 66 Model of Frontotemporal Dementia Demonstrates Actions on Tau-Dependent and Tau-Independent Networks. *Cells* **10**, 2162 (2021).

26. S. Gauthier, H. H. Feldman, L. S. Schneider, G. K. Wilcock, G. B. Frisoni, J. H. Hardlund, H. J. Moebius, P. Bentham, K. A. Kook, D. J. Wischik, B. O. Schelter, C. S. Davis, R. T. Staff, L. Bracoud, K. Shamsi, J. M. D. Storey, C. R. Harrington, C. M. Wischik, Efficacy and safety of tau-aggregation inhibitor therapy in patients with mild or moderate Alzheimer's disease: a randomised, controlled, double-blind, parallel-arm, phase 3 trial. *Lancet* **388**, 2873–2884 (2016).

27. G. K. Wilcock, S. Gauthier, G. B. Frisoni, J. Jia, J. H. Hardlund, H. J. Moebius, P. Bentham, K. A. Kook, B. O. Schelter, D. J. Wischik, C. S. Davis, R. T. Staff, V. Vuksanovic, T. Ahearn, L. Bracoud, K. Shamsi, K. Marek, J. Seibyl, G. Riedel, J. M. D. Storey, C. R. Harrington, C. M. Wischik, Potential of Low Dose Leuco-Methylthioninium Bis(Hydromethanesulphonate) (LMTM) Monotherapy for Treatment of Mild Alzheimer's Disease: Cohort Analysis as Modified Primary Outcome in a Phase III Clinical Trial. *J. Alzheimer's Dis.* **61**, 435–457 (2018).

28. B. O. Schelter, H. Shiells, T. C. Baddeley, C. M. Rubino, H. Ganesan, J. Hammel, V. Vuksanovic, R. T. Staff, A. D. Murray, L. Bracoud, G. Riedel, S. Gauthier, J. Jia, P. Bentham, K. Kook, J. M. D. Storey, C. R. Harrington, C. M. Wischik, Concentration-Dependent Activity of Hydromethylthionine on Cognitive Decline and Brain Atrophy in Mild to Moderate Alzheimer's Disease. *J. Alzheimer's Dis.* **72**, 931–946 (2019).

29. R. L. Buckner, A. Z. Snyder, B. J. Shannon, G. LaRossa, R. Sachs, A. F. Fotenos, Y. I. Sheline, W. E. Klunk, C. A. Mathis, J. C. Morris, M. A. Mintun, Molecular, structural, and functional characterization of Alzheimer's disease: Evidence for a relationship between default activity, amyloid, and memory. *J. Neurosci.* **25**, 7709–7717 (2005).

30. J. delEtoile, H. Adeli, Graph Theory and Brain Connectivity in Alzheimer's Disease. *Neuroscientist* **23**, 616–626 (2017).

31. S. Huang, J. Li, L. Sun, J. Liu, T. Wu, K. Chen, A. Fleisher, E. Reiman, J. Ye, Learning brain connectivity of Alzheimer's disease from neuroimaging data. *Adv. Neural Inf. Process. Syst. 22 - Proc. 2009 Conf.* , 808–816 (2009).

32. M. D. Seeley, W. W.; Crawford, R. K.; Zhou, J.; Miller, B. L.; Greicius, Neurodegenerative diseases target large-scale human brain networks. *Neuron* **62**, 42–52 (2009).

33. V. Vuksanović, R. T. Staff, T. Ahearn, A. D. Murray, C. M. Wischik, Cortical Thickness and Surface Area Networks in Healthy Aging, Alzheimer's Disease and Behavioral Variant Fronto-Temporal Dementia. *Int. J. Neural Syst.* **29**, 1–26 (2019).

34. J. Zhou, M. D. Greicius, E. D. Gennatas, M. E. Growdon, J. Y. Jang, G. D. Rabinovici, J. H. Kramer, M. Weiner, B. L. Miller, W. W. Seeley, Divergent network connectivity changes in behavioural variant frontotemporal dementia and Alzheimer's disease. *Brain* **133**, 1352–1367 (2010).

35. C. M. Henstridge, M. Tzioras, R. C. Paolicelli, Glial contribution to excitatory and inhibitory synapse loss in neurodegeneration. *Front. Cell. Neurosci.* **13**, 1–26 (2019).

36. J. Subramanian, J. C. Savage, M. È. Tremblay, Synaptic Loss in Alzheimer's Disease: Mechanistic Insights Provided by Two-Photon in vivo Imaging of Transgenic Mouse Models. *Front. Cell. Neurosci.* **14**, 1–13 (2020).

37. T. C. Südhof, Neurotransmitter release: The last millisecond in the life of a synaptic vesicle. *Neuron* **80**, 675–690 (2013).

38. S. E. Kwon, E. R. Chapman, Synaptophysin Regulates the Kinetics of Synaptic Vesicle Endocytosis in Central Neurons. *Neuron* **70**, 847–854 (2011).

39. S. H. Song, G. J. Augustine, Synapsin isoforms and synaptic vesicle trafficking. *Mol. Cells* **38**, 936–940 (2015).

40. J. Lautenschläger, C. F. Kaminski, G. S. Kaminski Schierle, α-synuclein – regulator of exocytosis, endocytosis, or both? *Trends Cell Biol.* **27**, 468–479 (2017).

41. J. Sun, L. Wang, H. Bao, S. Premi, U. Das, E. R. Chapman, S. Roy, Functional cooperation of α-synuclein and VAMP2 in synaptic vesicle recycling. *Proc. Natl. Acad. Sci. U. S. A.* **166**, 11113–11115 (2019).

42. J. Mertins, J. Finke, R. Sies, K. M. Rink, J. Hasenauer, T. Lang, The mesoscale organization of syntaxin 1A and SNAP25 is determined by SNARE-SNARE interactions. *Elife* **10**, 1–22 (2021).

43. N. P. du Sert, V. Hurst, A. Ahluwalia, S. Alam, M. T. Avey, M. Baker, W. J. Browne, A. Clark, I. C. Cuthill, U. Dirnagl, M. Emerson, P. Garner, S. T. Holgate, D. W. Howells, N. A. Karp, S. E. Lazic, K. Lidster, C. J. MacCallum, M. Macleod, E. J. Pearl, O. H. Petersen, F. Rawle, P. Reynolds, K. Rooney, E. S. Sena, S. D. Silberberg, T. Steckler, H. Würbel, The arrive guidelines 2.0: Updated guidelines for reporting animal research. *PLoS Biol.* **18**, 1–12 (2020).

44. V. Melis, C. Zabke, K. Stamer, M. Magbagbeolu, K. Schwab, P. Marschall, R. W. Veh, S. Bachmann, S. Deiana, P. H. Moreau, K. Davidson, K. A. Harrington, J. E. Rickard, D. Horsley, R. Garman, M. Mazurkiewicz, G. Niewiadomska, C. M. Wischik, C. R. Harrington, G. Riedel, F. Theuring, Different pathways of molecular pathophysiology underlie cognitive and motor tauopathy phenotypes in transgenic models for Alzheimer's disease and frontotemporal lobar degeneration. *Cell. Mol. Life Sci.* **72**, 2199–2222 (2015).

45. A. L. Cranston, A. Wysocka, M. Steczkowska, M. Zadrożny, E. Palasz, C. R. Harrington, F. Theuring, C. M. Wischik, G. Riedel, G. Niewiadomska, Cholinergic and inflammatory phenotypes in transgenic tau mouse models of Alzheimer's disease and frontotemporal lobar degeneration. *Brain Commun.* **2** (2020), doi:10.1093/braincomms/fcaa033.

46. R. J. Polinsky, Clinical pharmacology of rivastigmine: A new-generation acetylcholinesterase inhibitor for the treatment of Alzheimer's disease. *Clin. Ther.* **20**, 634–647 (1998).

47. C. Bejar, R. H. Wang, M. Weinstock, Effect of rivastigmine on scopolamine-induced memory impairment in rats. *Eur. J. Pharmacol.* **383**, 231–240 (1999).

48. D. Van Dam, D. Abramowski, M. Staufenbiel, P. P. De Deyn, Symptomatic effect of donepezil, rivastigmine, galantamine and memantine on cognitive deficits in the APP23 model. *Psychopharmacology (Berl).* **180**, 177–190 (2005).

49. C. Kondak, G. Riedel, C. R. Harrington, C. M. Wischik, J. Klein, Hydromethylthionine enhancement of central cholinergic signalling is blocked by rivastigmine and memantine. *J. Neurochem.* **160**, 172–184 (2022).

50. A. Nair, S. Jacob, A simple practice guide for dose conversion between animals and human. *J. Basic Clin. Pharm.* **7**, 27 (2016).

51. G. Paxinos, K. Franklin, *The mouse brain in stereotaxic coordinates* (Academic Press, 5th Editio., 2019).

52. S. Frahm, V. Melis, D. Horsley, J. E. Rickard, G. Riedel, P. Fadda, M. Scherma, C. R. Harrington, C. M. Wischik, F. Theuring, K. Schwab, Alpha-Synuclein transgenic mice, h-α-SynL62, display α-Syn aggregation and a dopaminergic phenotype reminiscent of Parkinson's disease. *Behav. Brain Res.* **339**, 153–168 (2018).

53. S. L. DeVos, B. T. Corjuc, D. H. Oakley, C. K. Nobuhara, R. N. Bannon, A. Chase, C. Commins, J. A. Gonzalez, P. M. Dooley, M. P. Frosch, B. T. Hyman, Synaptic tau seeding precedes tau pathology in human Alzheimer's disease brain. *Front. Neurosci.* **12**, 1–15 (2018).

54. J. Burré, W. Volknandt, The synaptic vesicle proteome. *J. Neurochem.* **101**, 1448–1462 (2007).

55. M. Morciano, T. Beckhaus, M. Karas, H. Zimmermann, W. Volknandt, The proteome of the presynaptic active zone: From docked synaptic vesicles to adhesion molecules and maxi-channels. *J. Neurochem.* **108**, 662–675 (2009).

56. M. Laßek, J. Weingarten, W. Volknandt, The synaptic proteome. *Cell Tissue Res.* **359**, 255–265 (2015).

57. R. S. Gormal, F. A. Meunier, Nanoscale organization of the pre-synapse: Tracking the neurotransmitter release machinery. *Curr. Opin. Neurobiol.* **75**, 102576 (2022).

58. E. Bulovaite, Z. Qiu, M. Kratschke, A. Zgraj, D. G. Fricker, E. J. Tuck, R. Gokhale, B. Koniaris, S. A. Jami, P. Merino-Serrais, E. Husi, L. Mendive-Tapia, M. Vendrell, T. J. O'Dell, J. DeFelipe, N. H. Komiyama, A. Holtmaat, E. Fransén, S. G. N. Grant, A brain atlas of synapse protein lifetime across the mouse lifespan. *Neuron* , 1–17 (2022).

59. M. C. De Wilde, C. R. Overk, J. W. Sijben, E. Masliah, Meta-analysis of synaptic pathology in Alzheimer's disease reveals selective molecular vesicular machinery vulnerability. *Alzheimer's Dement.* **12**, 633–644 (2016).

60. R. X. Santos, V. Melis, E. A. Goatman, M. Leith, T. C. Baddeley, J. M. D. Storey, G. Riedel, C. M. Wischik, C. R. Harrington, HMTM-Mediated Enhancement of Brain Bioenergetics in a Mouse Tauopathy Model Is Blocked by Chronic Administration of Rivastigmine. *Biomedicines* **10**, 1–21 (2022).

61. N. Lemke, V. Melis, D. Lauer, M. Magbagbeolu, B. Neumann, C. R. Harrington, G. Riedel, C. M. Wischik, F. Theuring, K. Schwab, Differential compartmental processing and phosphorylation of pathogenic human tau and native mouse tau in the line 66 model of frontotemporal dementia. *J. Biol. Chem.* **295**, 18508–18523 (2020).

62. Y. C. Li, E. T. Kavalali, Synaptic vesicle-recycling machinery components as potential therapeutic targets. *Pharmacol. Rev.* **69**, 141–160 (2017).

63. M. Robbins, E. Clayton, G. S. Kaminski Schierle, Synaptic tau: A pathological or physiological phenomenon? *Acta Neuropathol. Commun.* **9**, 1–30 (2021).

64. L. Zhou, J. McInnes, K. Wierda, M. Holt, A. G. Herrmann, R. J. Jackson, Y. C. Wang, J. Swerts, J. Beyens, K. Miskiewicz, S. Vilain, I. Dewachter, D. Moechars, B. De Strooper, T. L. Spires-Jones, J. De Wit, P. Verstreken, Tau association with synaptic vesicles causes presynaptic dysfunction. *Nat. Commun.* **8**, 1–13 (2017).

65. J. McInnes, K. Wierda, A. Snellinx, L. Bounti, Y. C. Wang, I. C. Stancu, N. Apóstolo, K. Gevaert, I. Dewachter, T. L. Spires-Jones, B. De Strooper, J. De Wit, L. Zhou, P. Verstreken, Synaptogyrin-3 Mediates Presynaptic Dysfunction Induced by Tau. *Neuron* **97**, 823-835.e8 (2018).

66. L. J. Agostinelli, J. C. Geerling, T. E. Scammell, Basal forebrain subcortical projections. *Brain Struct. Funct.* **224**, 1097–1117 (2019).

67. E. E. Hur, R. H. Edwards, E. Rommer, L. Zaborszky, Vesicular glutamate transporter 1 and vesicular glutamate transporter 2 synapses on cholinergic neurons in the sublenticular gray of the rat basal forebrain: a double-label electron microscopic study. *Neuroscience* **164**, 1721–1731 (2009).

68. K. Toth, Z. Borhegyi, T. F. Freund, Postsynaptic targets of GABAergic hippocampal neurons in the medial septum-diagonal band of Broca complex. *J. Neurosci.* **13**, 3712–3724 (1993).

69. S. Jinno, T. Kosaka, Immunocytochemical characterization of hippocamposeptal projecting GABAergic nonprincipal neurons in the mouse brain: A retrograde labeling study. *Brain Res.* **945**, 219–231 (2002).

70. X. Wu, W. Morishita, K. T. Beier, B. D. Heifets, R. C. Malenka, 5-HT modulation of a medial septal circuit tunes social memory stability. *Nature* **599**, 96–101 (2021).

71. Q. Sun, J. Zhang, A. Li, M. Yao, G. Liu, S. Chen, Y. Luo, Z. Wang, H. Gong, X. Li, Q. Luo, Acetylcholine deficiency disrupts extratelencephalic projection neurons in the prefrontal cortex in a mouse model of Alzheimer's disease. *Nat. Commun.* **13** (2022), doi:10.1038/s41467-022-28493-4.

72. M. M. Paul, S. Dannhäuser, L. Morris, A. Mrestani, M. Hübsch, J. Gehring, G. N. Hatzopoulos, M. Pauli, G. M. Auger, G. Bornschein, N. Scholz, D. Ljaschenko, M. Müller, M. Sauer, H. Schmidt, R. J. Kittel, A. DiAntonio, I. Vakonakis, M. Heckmann, T. Langenhan, The human cognition-enhancing CORD7 mutation increases active zone number and synaptic release. *Brain* (2022), doi:10.1093/brain/awac011.

73. G. Riedel, Function of metabotropic glutamate receptors in learning and memory. *Trends Neurosci.* **19**, 219–224 (1996).

74. S. Grossman, E. M. Yeagle, M. Harel, E. Espinal, R. Harpaz, N. Noy, P. Mégevand, D. M. Groppe, A. D. Mehta, R. Malach, The Noisy Brain: Power of Resting-State Fluctuations Predicts Individual Recognition Performance. *Cell Rep.* **29**, 3775-3784.e4 (2019).

75. D. A. Rusakov, L. P. Savtchenko, P. E. Latham, Noisy Synaptic Conductance: Bug or a Feature? *Trends Neurosci.* **43**, 363–372 (2020).

76. G. Marucci, M. Buccioni, D. D. Ben, C. Lambertucci, R. Volpini, F. Amenta, Efficacy of acetylcholinesterase inhibitors in Alzheimer's disease. *Neuropharmacology* **190** (2021), doi:10.1016/j.neuropharm.2020.108352.

77. S. Matsunaga, H. Fujishiro, H. Takechi, Efficacy and Safety of Cholinesterase Inhibitors for Mild Cognitive Impairment:A Systematic Review and Meta-Analysis. *J. Alzheimer's Dis.* **71**, 513–523 (2019).

78. E. Bereczki, P. T. Francis, D. Howlett, J. B. Pereira, K. Höglund, A. Bogstedt, A. Cedazo-Minguez, J. H. Baek, T. Hortobágyi, J. Attems, C. Ballard, D. Aarsland, Synaptic proteins predict cognitive decline in Alzheimer's disease and Lewy body dementia. *Alzheimer's Dement.* **12**, 1149–1158 (2016).

79. J. N. K. Nyarko, M. O. Quartey, R. M. Heistad, P. R. Pennington, L. J. Poon, K. J. Knudsen, O. Allonby, A. M. El Zawily, A. Freywald, G. Rauw, G. B. Baker, D. D. Mousseau, Glycosylation states of pre- and post-synaptic markers of 5-HT neurons differ with sex and 5-HTTLPR genotype in cortical autopsy samples. *Front. Neurosci.* **12**, 1–17 (2018).

80. E. Gkanatsiou, J. Nilsson, C. E. Toomey, A. Vrillon, H. Kvartsberg, E. Portelius, H. Zetterberg, K. Blennow, A. Brinkmalm, T. Lashley, G. Brinkmalm, Amyloid pathology and synaptic loss in pathological aging. *J. Neurochem.* **159**, 258–272 (2021).

81. A. Ramos-Miguel, A. A. Jones, K. Sawada, A. M. Barr, T. A. Bayer, P. Falkai, S. E. Leurgans, J. A. Schneider, D. A. Bennett, W. G. Honer, Frontotemporal dysregulation of the SNARE protein interactome is associated with faster cognitive decline in old age. *Neurobiol. Dis.* **114**, 31–44 (2018).

82. E. B. Mukaetova-Ladinska, F. Garcia-Siera, J. Hurt, H. J. Gertz, J. H. Xuereb, R. Hills, C. Brayne, F. A. Huppert, E. S. Paykel, M. McGee, R. Jakes, W. G. Honer, C. R. Harrington, C. M. Wischik,

Staging of cytoskeletal and β-amyloid changes in human isocortex reveals biphasic synaptic protein response during progression of Alzheimer's disease. *Am. J. Pathol.* **157**, 623–636 (2000).

83. L. Zhou, J. McInnes, K. Wierda, M. Holt, A. G. Herrmann, R. J. Jackson, Y. C. Wang, J. Swerts, J. Beyens, K. Miskiewicz, S. Vilain, I. Dewachter, D. Moechars, B. De Strooper, T. L. Spires-Jones, J. De Wit, P. Verstreken, Tau association with synaptic vesicles causes presynaptic dysfunction. *Nat. Commun.* **8** (2017), doi:10.1038/ncomms15295.

Graphical abstract

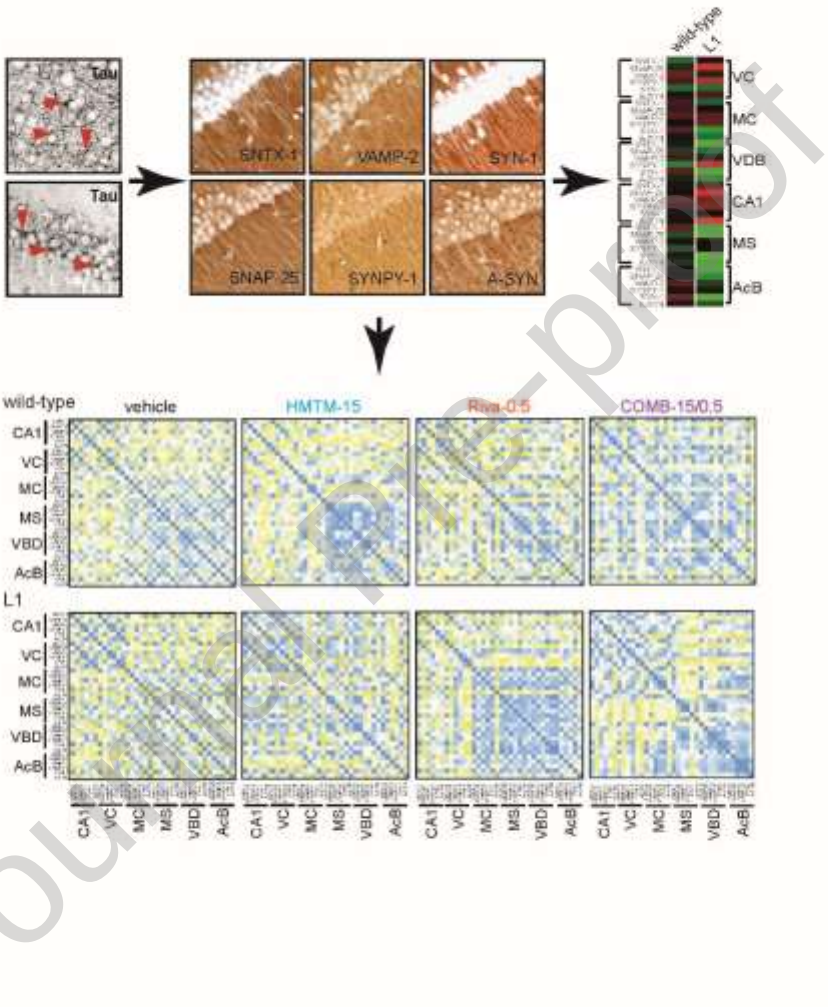

Highlights

- Interference of cholinesterase inhibition with HMTM was observed in AD clinical trials.
- The interference on expression of pre-synaptic proteins was investigated in L1 mice.
- L1 mice overexpress tau that leads to dysregulation of synaptic proteins.
- HMTM alone partially normalised the expression pattern of several of these proteins.
- The effect was diminished when HMTM was administered in combination with rivastigmine.